AGU PUBLICATIONS

JGR

Journal of Geophysical Research: Solid Earth

RESEARCH ARTICLE
10.1002/2017JB014487

Neotectonic Deformation in Central Eurasia: A Geodynamic Model Approach

Lavinia Tunini[1,2], Ivone Jiménez-Munt[1], Manel Fernandez[1], Jaume Vergés[1], and Peter Bird[3]

[1]Group of Dynamics of the Lithosphere, Institute of Earth Sciences Jaume Almera, CSIC, Barcelona, Spain, [2]Now at Ecole Normale Supérieure, Department of Geosciences, Paris, France, [3]Department of Earth, Planetary, and Space Sciences, University of California, Los Angeles, CA, USA

Key Points:
- Modeled velocities reproduce lateral escape tectonics due to the continental collisions of Arabia and India with Eurasia
- SE Tibet velocities can be explained by the combination of Sumatra trench retreat, a lithospheric mantle thinning and strike-slip faulting
- Arabia-India intercollision zone shows no velocity deflections related to Arabia and India indentations

Correspondence to:
L. Tunini,
lavinia.tunini@ens.fr

Citation:
Tunini, L., Jiménez-Munt, I., Fernandez, M., Vergés, J., & Bird, P. (2017). Neotectonic deformation in central Eurasia: A geodynamic model approach. *Journal of Geophysical Research: Solid Earth*, *122*. https://doi.org/10.1002/2017JB014487

Received 29 MAY 2017
Accepted 9 NOV 2017
Accepted article online 12 NOV 2017

Abstract Central Eurasia hosts wide orogenic belts of collision between India and Arabia with Eurasia, with diffuse or localized deformation occurring up to hundreds of kilometers from the primary plate boundaries. Although numerous studies have investigated the neotectonic deformation in central Eurasia, most of them have focused on limited segments of the orogenic systems. Here we explore the neotectonic deformation of all of central Eurasia, including both collision zones and the links between them. We use a thin-spherical sheet approach in which lithosphere strength is calculated from lithosphere structure and its thermal regime. We investigate the contributions of variations in lithospheric structure, rheology, boundary conditions, and fault friction coefficients on the predicted velocity and stress fields. Results (deformation pattern, surface velocities, tectonic stresses, and slip rates on faults) are constrained by independent observations of tectonic regime, GPS, and stress data. Our model predictions reproduce the counterclockwise rotation of Arabia and Iran, the westward escape of Anatolia, and the eastward extrusion of the northern Tibetan Plateau. To simulate the observed extensional faults in the Tibetan Plateau, a weaker lithosphere is required, provided by a change in the rheological parameters. The southward movement of the SE Tibetan Plateau can be explained by the combined effects of the Sumatra trench retreat, a thinner lithospheric mantle, and strik-slip faults in the region. This study offers a comprehensive model for regions with little or no data coverage, like the Arabia-India intercollision zone, where the surface velocity is northward showing no deflection related to Arabia and India indentations.

1. Introduction

Central Eurasia hosts one of the most outstanding topographic features on Earth: a huge Cenozoic mountain belt spans from eastern Turkey to central China (Figure 1). This belt includes the Zagros mountains, the Himalaya range, the Tibetan Plateau, and surrounding ranges, and it is the result of the continental collisions between the Arabia and India plates and the southern margin of the Eurasia plate, triggered by the subduction of the Tethys oceanic lithosphere beneath Eurasia.

Continental collision is still active, as manifested by significant seismicity, fault slip rates, and GPS velocities (Figure 2) (Bettinelli et al., 2006; Burgess et al., 2012; Gan et al., 2007; Khodaverdian, Zafarani, & Rahimian, 2015; Mousavi, 2016; Raeesi et al., 2016; Reilinger et al., 2006; Socquet et al., 2006; Vernant et al., 2004; Vigny et al., 2003; Walpersdorf et al., 2014; Zarifi, Nilfouroushan, & Raeesi, 2013). The deformation is not only localized around plate margins but is diffused up to hundreds of kilometers away from the suture zones. At lithospheric scale, the deformation has caused lateral and in-depth variations of lithospheric-crustal thickness, density, temperature, and composition, as revealed by recent studies combining geophysical, thermal, and/or petrological data (Robert et al., 2015; Tunini et al., 2015, 2016). These differences produce lithospheric body forces and deviatoric stresses and directly affect the strength of the lithosphere.

The strength heterogeneities distributed laterally and in depth within the crust and lithosphere are key parameters for understanding and modeling the mode and localization of the deformation (Cook & Royden, 2008). The spreading or migration of the mountain belts and the surface velocities are strongly affected by the strength of the crustal rocks, the presence of embedded rigid blocks, and upper mantle processes (e.g., subductions, slab-tears, and slab breakoffs) (Calignano et al., 2015; Capitanio, 2014; Ghosh et al., 2006).

Tectonics in central Eurasia (Figure 1) features subducting slabs in the eastern Anatolia (Rizaoglu et al., 2009; Sengör et al., 2003), Pamir (Li et al., 2008; Negredo et al., 2007), Makran (Byrne, Sykes, & Davis, 1992), and Burma (Huang & Zhao, 2006; Li et al., 2008) regions; rigid aseismic blocks (central Iran, Lut, Afghan block,

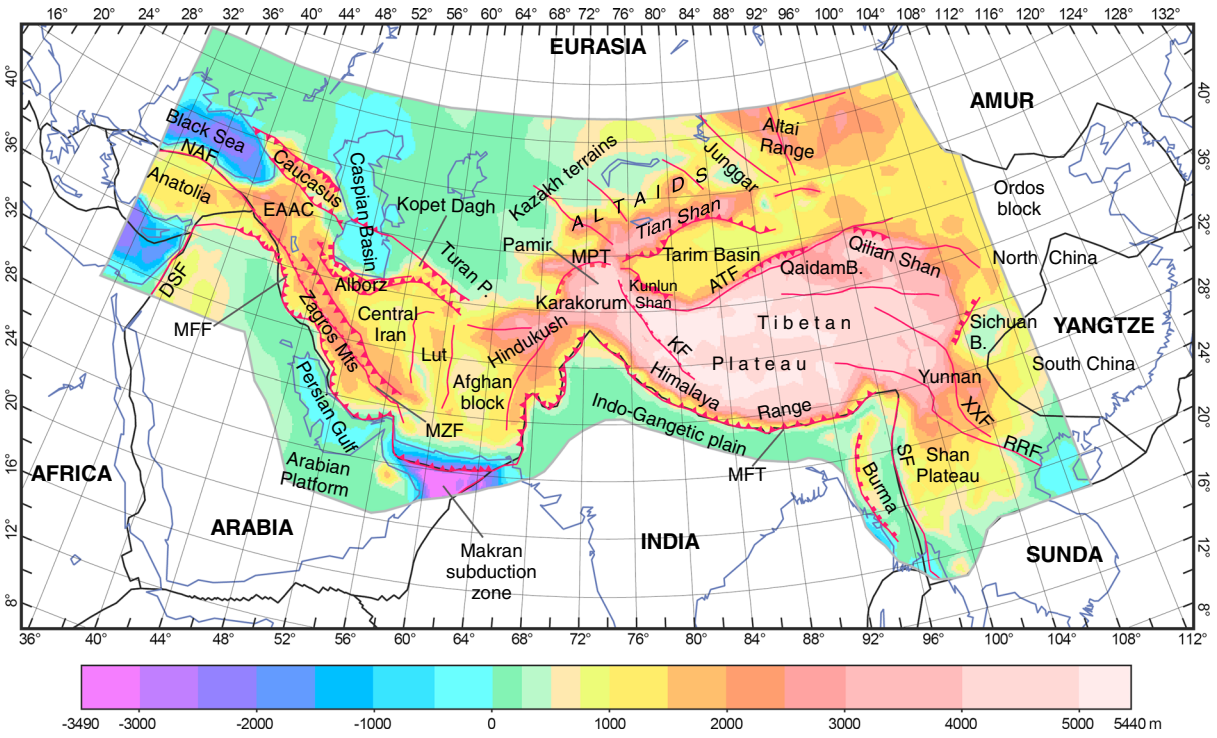

Figure 1. Topography (from ETOPO1 model; Amante & Eakins, 2009) and tectonic settings of central Eurasia. The black thin lines indicate plate boundaries from PB2002 plate model (Bird, 2003). ATF: Altyn Tagh fault; DSF: Dead Sea fault; EAAC: Eastern Anatolia accretionary complex; KF: Karakorum fault; MFT: Main Frontal thrust; MFF: Mountain Front Flexure; MPT: Main Pamir thrust; MZF: Main Zagros fault; NAF: North Anatolia fault; RRF: Red River fault; SF: Sagaing fault; XXF: Xiangshuihe-Xiaojiang fault.

Tarim basin, and Sichuan basin); large-scale fault zones; or major preexisting structures derived from the amalgamation of Gondwana-derived continental blocks (e.g., Audet & Bürgmann, 2011). The presence of indenters, the NW and NE corners of India, delineating the Bramaputra and Nanga Parbat syntaxes, and the NW border of Arabia, may be sites of partial slab breakoff at depth (Capitanio, 2014).

Several authors have investigated the neotectonic deformation of central Eurasia. A viscous thin-sheet model of Iran showed that the presence of rigid blocks, i.e., central Iran and the South Caspian basin, primarily control the deformation, the observed crustal thickness, and the faulting patterns (Sobouti & Arkani-Hamed, 1996). The same methodology was applied in the India-Eurasia collision zone and south-eastern Asia by Vergnolle, Calais, and Dong (2007). Their results show that in the mountain belts surrounding the Tibetan Plateau, i.e., Himalayas, Tian Shan, and Altai range, the deformation could be well reproduced with strong coupling at the India/Eurasia plate contact, which allows the stresses to be transferred to the interior of Asia. However, south-eastward motions observed in south-eastern China block require tensional, oceanward directed stresses, generated by gravitational potential energy (GPE) gradients from the high orogen to the deep trenches of the Indonesian and Pacific subductions (Vergnolle et al., 2007). Lechmann et al. (2014) investigated the effects of lithosphere layering on the deformation in the India-Asia collision, and they found that the viscous stresses are consistent with GPE-induced stresses. Their best results are obtained with a weak Sagaing fault.

These studies provide reliable insights into the deformation within the Arabia-Eurasia and India-Eurasia collision zones. However, they only focus on one of the collisions (Arabia-Eurasia or India-Eurasia), not being able to study the interaction between the two of them.

We investigate the neotectonic deformation of the whole of central Eurasia (Figure 1), including both the Arabia-Eurasia and India-Eurasia collisions. We adopt a geodynamic modeling technique based on the thin-spherical-shell approximation, which allows inferring the surface velocity field, stress directions, tectonic regime, and strain distribution by imposing velocity boundary conditions on a model domain simulating a faulted lithosphere on a spherical Earth. We investigate the relative contributions of the lithospheric

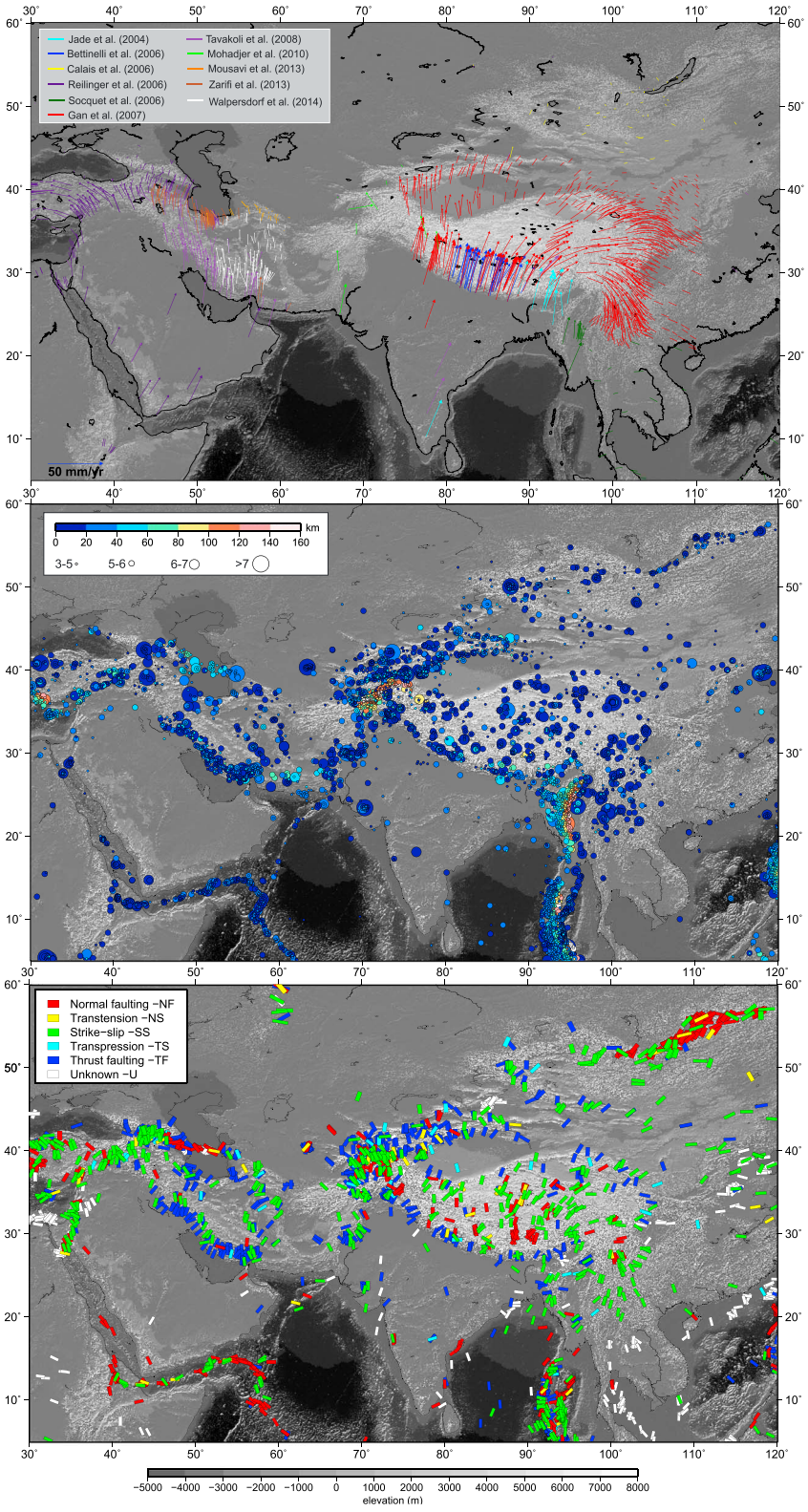

Figure 2. (a) GPS velocities in the Eurasia reference frame. (b) Earthquake distribution ($M > 3$) (Engdahl, van der Hilst, & Buland, 1998). The colors indicate the depth of the hypocenters and the size indicates the magnitude. (c) Stress data compilation from the World Stress Map WSM2008 (Heidbach et al., 2008). The lines show the directions of the most-compressive horizontal principal stress axis, and the colors show the tectonic regime. Data have been filtered to quality C (stress orientations are accurate to within 25°) or better, and depths less than 50 km.

structure, rheology, boundary conditions, and friction coefficient on faults on the predicted velocity and stress fields. The lithosphere strength is calculated from the lithosphere structure and the associated thermal regime. We use the recent crustal and lithospheric structure model by Robert et al. (2015) and the results from Jiménez-Munt et al. (2008) and Tunini et al. (2015 and 2016). The thin-sheet approach has proven to be useful for studying both the present-day (neotectonic) deformation in collisional settings (Barba et al., 2010; Bird, Liu, & Rucker, 2008; Cunha et al., 2012; England & Molnar, 1997; Howe & Bird, 2010; Jiménez-Munt et al., 2001, 2003; Liu & Bird, 2002; Marotta et al., 2001; Negredo et al., 2002; Negredo, Jiménez-Munt, & Villaseñor, 2004; Neres et al., 2016) and its evolution through time (England & Housemann, 1989; Garcia-Castellanos & Jiménez-Munt, 2015; Jiménez-Munt, Garcia-Castellanos, & Fernandez, 2005; Jiménez-Munt & Platt, 2006; Robl & Stüwe, 2005; Sobouti & Arkani-Hamed, 1996; Sternai et al., 2016).

We explore different potential scenarios in order to explain the observations (GPS velocity, stress direction, and seismic deformation) in both Arabia-Eurasia and India-Eurasia collision zones and to provide new insights in the Pakistan and Afghanistan regions, which are poorly understood because there is little or no data coverage. We study the effect of changing the lithosphere structure on the resulting surface velocities and tectonic stresses. We show a model based on a thick crust and a thick lithospheric mantle to maintain the height of the Tibetan Plateau. We also discuss the results of a model with a thinner lithospheric mantle beneath the northeast Tibetan Plateau, which has been proposed in order to explain seismic tomography models and potential field data (references in Jiménez-Munt et al., 2008, and Tunini et al., 2016). Changes in the rheological parameters, friction coefficient on faults, and velocity conditions at boundary nodes are applied to see their effects on the predicted velocity, stress orientations, and tectonic regime. The models are evaluated by comparing the predictions with available data on seismic deformation, stress directions, and GPS velocities.

2. Tectonic and Geodynamic Context

Central Eurasia contains two of the most prominent deformed regions on Earth: the Arabia-Eurasia and the India-Eurasia collision zones. The strong and resistant Archean-to-Proterozoic shields of the Arabia and India plates collided during the Cenozoic with the complex mosaic structure of the ancient Eurasian margin, which was formed from different Gondwana-derived continental blocks accreted by Late-Mesozoic time.

The Arabia plate originated ~25 Ma when rifting to form the Gulf of Aden and the Red Sea split off a fragment of the Nubia plate. Drifting to the north, the Arabia plate collided with the southern border of the Eurasia plate, where the Neotethyan oceanic lithosphere had been subducting beneath Eurasia since the Late Cretaceous (e.g., McQuarrie & van Hinsbergen, 2013; Mouthereau, Lacombe, & Vergés, 2012; Vergés et al., 2011). Associated uplift and mantle processes resulted in a gentle tilt of the Arabia plate toward the northeast, which exposed the Precambrian basement along its SW margin. The crystalline basement is overlain by a thick succession of Phanerozoic sedimentary rocks and Cenozoic basalts (Stern & Johnson, 2008, 2010). Basement and sedimentary rocks were involved in the compression, which resulted in the formation of the Zagros Mountains, a fold-thrust belt extending from eastern Turkey to the Hormuz Strait (Casciello et al., 2009; Emami et al., 2010; Sepehr & Cosgrove, 2004; Sherkati, Letouzey, & Frizon de Lamotte, 2006). The plate suture is located along the Main Zagros fault, which separates the Arabian domains from the Sanandaj Sirjan zone, an Iranian continental block with Palaeozoic to Cretaceous sedimentary and metamorphic rocks. The central Iran basin (east Iran) is filled by a 6–8 km thick Neogene sedimentary succession above Eocene volcanics and Cretaceous and Jurassic rocks (Morley et al., 2009). The Alborz range formed to the north of the central Iran basin along the Paleotethyan suture (Berberian & King, 1981; Robert et al., 2014; Sengör et al., 1988). The Alborz is bounded to the north by the South Caspian basin, an aseismic block characterized by more than 17 km thick Oligocene-Recent sedimentary succession, mildly folded and thrusted as a result of the Arabian-Eurasia collision (Egan et al., 2009). In north-west Iran, the northward subduction of the Neotethyan oceanic lithosphere beneath the Bitlis-Poturge massif (Rizaoglu et al., 2009; Sengör et al., 2003) formed the Eastern Anatolian accretionary complex (EAAC; Figure 1) and led to the onset of slip along the East Anatolia fault and the postcollisional volcanism in eastern Anatolia (Keskin, 2003). The North Anatolia fault zone formed in late Miocene-early Pliocene in response to a slab-detachment event (Faccenna et al., 2006), which is thought also to have modified the stress regime of the region, which changed from compression to transpression-transtension (Avagyan et al., 2010). The Caucasus range extends between the oceanic

rigid blocks of the Black Sea and Caspian Sea. It is composed of two fold-thrust belts (Lesser Caucassus and Greater Caucasus) separated by an intermontane depression and formed by the inversion of back-arc basins related to the Arabia-Africa collision with Eurasia (Adamia et al., 2011).

The India plate separated from Australia, Antarctica, and Madagascar and drifted toward the north as the consequence of Gondwana fragmentation ~140 Ma (Kumar et al., 2007). The northern drift culminated between 55 and 45 Ma with the continental collision with Eurasia forming the Himalaya-Tibet orogenic system (Hatzfeld & Molnar, 2010). Currently, the India plate is a mosaic of various Precambrian tectonic domains, assembled between mid-Archean and Neo-Proterozoic times (Braun & Kriegsmann, 2003; Meert et al., 2010). The Himalaya range corresponds to the ancient northern margin of the Indian continent, thrusted and folded in three major tectonic thrust sheets separated by major crustal thrusts: (1) the Indus-Tsangpo suture, representing the suture zone between India and Eurasia; (2) the Main Central thrust; and (3) the Main Boundary thrust. The Tibetan Plateau is a high terrain (average topography of 5 km) located to the north of the Himalaya range. It is the result of the progressive accretion of different tectonic blocks to the southern margin of Eurasia during the Phanerozoic. The Tarim basin is the largest cratonic area of western China, interpreted as a fragment of the Rodinia supercontinent (Lu et al., 2008, and references therein). Its Precambrian crystalline basement is overlied by a 4–12 km thick sedimentary sequence containing Ordovician, Permian, and Cretaceous strata (Gao & Ye, 1997). The Permian strata consist of volcano-sedimentary sequences related to the flood basalt magmatism that affected the so-called Tarim large igneous province ~290 Ma. Despite the Permian magmatic event, the evolution of the Tarim basin is characterized by almost continuous sedimentation since the Neo-Proterozoic (Xu et al., 2014).

The Afghan block, the Makran subduction zone, and the Hindukush are the most significant structures between the Arabia-Eurasia and India-Eurasia collision zones. This deformed zone is limited between the NNW trending right-slip Sistan and the left-slip Chaman fault systems. These two fault systems accommodate the northward propagation of Arabia (Bonini et al., 2003; Yin, 2009) and India into Eurasia, respectively. The Afghan block collided with India in late Cenozoic (~5 Ma) and was extruded westward along the conjugate Herat and Chaman strike-slip faults (Tapponnier et al., 1981). The Afghan block is bounded to the south by the Makran accretionary prism zone and to the north by the Pamir-Hindukush mountains. The Makran accretionary prism formed during the Paleogene and is still active above the north dipping oceanic subduction of the Arabia plate along the northern segment of the Oman Sea (Byrne et al., 1992). The Pamir region, located north of the western Himalayan syntaxis, accommodated a large amount of crustal shortening over a short north-south distance during the Cenozoic (Schmidt et al., 2011; van Hinsbergen et al., 2011). Further north, the Pamir thrusted over the Tajik-Afghan basin connected to the Tarim basin. Currently, an intense intermediate-depth seismicity (~90–250 km) beneath the Pamir and Hindukush ranges testifies to active geodynamic processes in the mantle (Schurr et al., 2014). The Turan platform and the Kazakh terrane are parts of the Eurasia plate. Their boundaries are defined by the extent of the Upper Permian to Quaternary deposits, which in the case of the Turan area overstep the south-western part of the Altaids mountains. The northernmost elevated terranes of Kazakhstan are affected by denudation processes since 3 Ma related to the India-Eurasia collision (Smit et al., 2013, and references therein).

3. Method

To simulate the neotectonic deformation in central Eurasia related to its continental collision with Arabia and India, we adopt a dynamic modeling approach using the numerical code SHELLS (Bird et al., 2008). The code solves the stress equilibrium equation for a spherical finite element grid, using vertically integrated stresses derived from laterally varying lithospheric structure and kinematic boundary conditions. This forward-modeling method calculates the velocity field, stress directions, tectonic regime, and strain rate distribution, assuming a defined lithosphere structure.

SHELLS is based on the thin-spherical-shell approximation, which allows the deformation of the lithosphere to be treated in terms of vertically averaged magnitudes, e.g., vertical integrated viscosity or stress (see Bird et al., 2008). The deformation can be accommodated by slip along faults (defined with a lower coefficient of friction and double nodes) and/or by distributed straining. Spatial variations in crust and lithospheric thickness induce lateral variations in gravitational potential energy (GPE), which in turn contribute to the force balance driving deformation. The thin spherical shell approach is thus suitable to investigate the deformation in

heterogeneous collisional settings such central Eurasia, where GPE differences could be significant. Flesch, Haines, and Holt (2001) showed that GPE contributes ~50% of the present-day deformation in Asia.

SHELLS is designed for neotectonic studies, and the timescale considered in the modeling is much larger than that of the earthquake cycle; therefore, transient effects such as elastic strain are neglected. Model outputs should be considered as averages over several seismic cycles. A 2-D finite element grid of spherical triangles is used to solve only the horizontal components of the momentum equation, whereas the radial (vertical) component of the momentum equation is represented by the isostatic approximation. The method can also be considered as "2.5-dimensional" since it performs volume integrals of density and strength in a lithosphere model with laterally varying thickness of the crust and mantle-lithosphere, heat flow, and topography.

The temperature distribution is calculated considering only the vertical component of the heat conduction and solving the thermal equation in 1-D. The lithosphere strength is calculated from the lithosphere structure and thermal regime assuming a nonlinear rheology.

The lithosphere is two-layered (crust and lithospheric mantle), and for each layer the rheology is assumed rigid plastic at low temperatures (Mohr-Coulomb-Navier friction) and deforms by power law creep at high T and P. Different constants are assumed for the quartz-diorite-dominated (feldspar-dominated) crust and dunite-dominated (olivine-dominated) mantle lithosphere (for details on SHELLS rheology please refer to Bird & Piper, 1980; Bird, 1999; and Carafa & Barba, 2011). Faults are designed as double-node linear elements of known dip within the grid and are characterized by the same rheology as continuum elements except for a lower friction coefficient. We use the SHELLS code (described in Bird et al., 2008), which considers elevation, heat flow, crustal thickness, and lithospheric mantle thickness as input data at each node of the finite element grid. Additionally, the program allows for two extra degrees of freedom at each node in order to fit seismically determined layer thicknesses: a perturbation of the geotherm away from steady state and an anomaly in the vertically averaged density of the lithosphere (limited to the range of ±50 kg/m^3; Bird et al., 2008). These two extra data are interpreted, respectively, as transient effects in the thermal state of the lithosphere and as compositional variations within the lithosphere. They are necessary in order to preserve local isostasy while fixing crust and lithosphere thicknesses, elevation, and surface heat flow to independent constraints.

In SHELLS, the model setup is essentially defined by the following inputs: (1) the model domain in map view, i.e., the finite element grid formed by triangular spherical elements and linear fault elements, and the dips of the active (or potentially active) faults; (2) the lithosphere structure, i.e., the crust and lithospheric mantle thicknesses; (3) the elevation and surface heat flow; (4) the density, rheology, and thermal parameters for the crust and lithospheric mantle; and (5) the velocities or forces applied as boundary conditions.

4. Model Setup

The two-dimensional finite element grid consists of fault elements and continuum elements. Fault elements are defined by double nodes, by the dip and a lower friction coefficient (μ_f) with respect to the continuum elements, which have a friction coefficient of 0.85. In this study, the finite element grid consists of 4,467 continuum elements and 435 fault elements (Figure 3). We used the traces of major active faults in the Altai range as reported by Holt et al. (2000), in the Himalaya-Tibet region by Taylor and Yin (2009), and in the rest of the area we referred to Bonini et al. (2003), Liu and Bird (2008), and references therein. Fault dips are assigned on the basis of available dip data or from geological cross sections (Ballato & Strecker, 2014; Burchfiel et al., 2008; Burg et al., 2008; Charvet et al., 2011; Guillot et al., 2003; Li et al., 2011; Mosar et al., 2010; Robert et al., 2009, 2014; Saura et al., 2011; Yin, 2006): 20–35° for compressional faults, 60–70° for extensional faults, and 90° for strike-slip faults (Figure 3). The subduction megathrust faults in the Arabia-Eurasia collision (Mountain Front Flexure (MFF) and Makran subduction) and the India-Eurasia collision (Main Frontal thrust (MFT)) are considered to have a lower strength. On these faults, the vertical integral of the shear traction is limited to a certain value (TAUMAX in Table 3; for more details see Bird et al., 2008). This special treatment, which has been found to be useful in previous modeling studies, can be justified by the likelihood of permanent superhydrostatic pore pressures in fast-sliding subduction megathrusts.

4.1. Lithosphere Structure

The lithospheric structure used in this study comes from the central Eurasia lithospheric model by Robert et al. (2015), resulting from the combination of elevation, geoid anomaly, and thermal analysis (Figure 4).

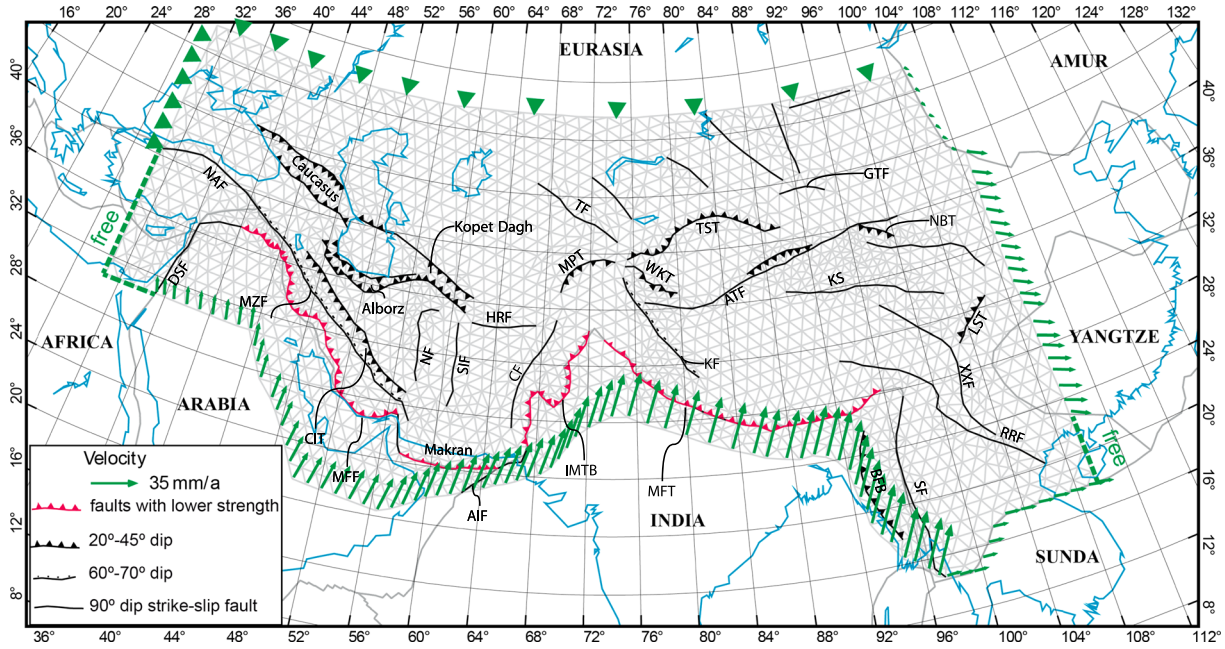

Figure 3. Finite element grid and boundary conditions of the reference model: (1) fixed Eurasia plate all along the northern boundary of the model and north of 40.4°N in the western border (thick triangles); (2) "free velocity" along the SW and SE corners (dashed lines), where normal tractions are equal to the lithostatic vertical stresses; and (3) imposed boundary velocities according to the Euler poles in Table 1 (green arrows). Fault traces are shown in black and red, coastline in blue. Tectonic plate boundaries are shown in thin grey lines. AIF: Arabia-India transform Fault; ATF: Altyn Tagh fault; BFF: Burmese fold belt; CF: Chaman fault; CIT: Central Iran thrust; DSF: Dead Sea fault; GTF: Gobi-Tian Shan fault; HRF: Herat fault; IMTB: Indus-Makran thrust belt; KF: Karakorum fault; KS: Kunlun suture (or Kunlun fault); LST: Longmen Shan thrust; MFT: Main Frontal thrust; MFF: Mountain Front Flexure; MPT: Main Pamir thrust; MZF: Main Zagros fault; NAF: North Anatolia fault; NBT: North Border thrust; NF: Nayband fault; RRF: Red River fault; SF: Sagaing fault; SIF: Sistan fault; TF: Talas-Fergana fault; TST: Tian Shan thrust; WKT: Western Kunlun thrust; XXF: Xiangshuihe-Xiaojiang fault.

Their results are also constrained by numerous previous data based on seismological and seismic experiments, tomographic imaging, and integrated geophysical studies.

The model shows that crustal thickening extends hundreds to thousand kilometers away from the collisional front, indicating transmission of tectonic stresses, and revealing the presence of stiff lithospheric blocks that remain almost undeformed within the collisional systems (central Iran, Tarim basin). The front of the Zagros Mountains is characterized by ~200 km thick lithosphere, and the internal regions of Anatolia, central Iran, Alborz, and Lut block by a 100–130 km thick lithosphere, in agreement with previous studies (Jiménez-Munt et al., 2012; Molinaro, Zeyen, & Laurencin, 2005; Motavalli-Anbaran et al., 2011; Tunini et al., 2015).

The India-Eurasia collision zone shows a thicker lithosphere with respect to the Arabia-Eurasia region (>200 km thick). In the north-eastern Tibetan Plateau maximum values of 340 km are calculated in contrast to previous geophysical studies and tomography images, which suggest a very thin to absent lithospheric mantle in this region (Jiménez-Munt et al., 2008; Kumar et al., 2006; Liang et al., 2012; Tunini et al., 2016; Zhao et al., 2010). This discrepancy is discussed in detail by Robert et al. (2015).

4.2. Boundary Conditions

Deformation in central Asia is mainly dominated by the collision of Arabia and India with Eurasia. However, six major plates intersect in the central Eurasia region: Eurasia, Arabia, India, Sunda, Yangtze, and Amur (see Figure 1). In this work Eurasia is considered the reference plate and then, all the other plate velocities are referred to it.

Several studies have constrained the relative velocity between the different plates as a rotation around an Euler pole (Argus et al., 2010; Bird, 2003; DeMets et al., 1990; DeMets, Gordon, & Argus, 2010; Liu & Bird, 2008). We define the velocity boundary conditions according to these relative motions between plates. We have experimented with Euler poles from different authors, but here we only present the results from Liu and Bird (2008) (Table 1 and Figure 3) since they provide the best fits between our model-predicted

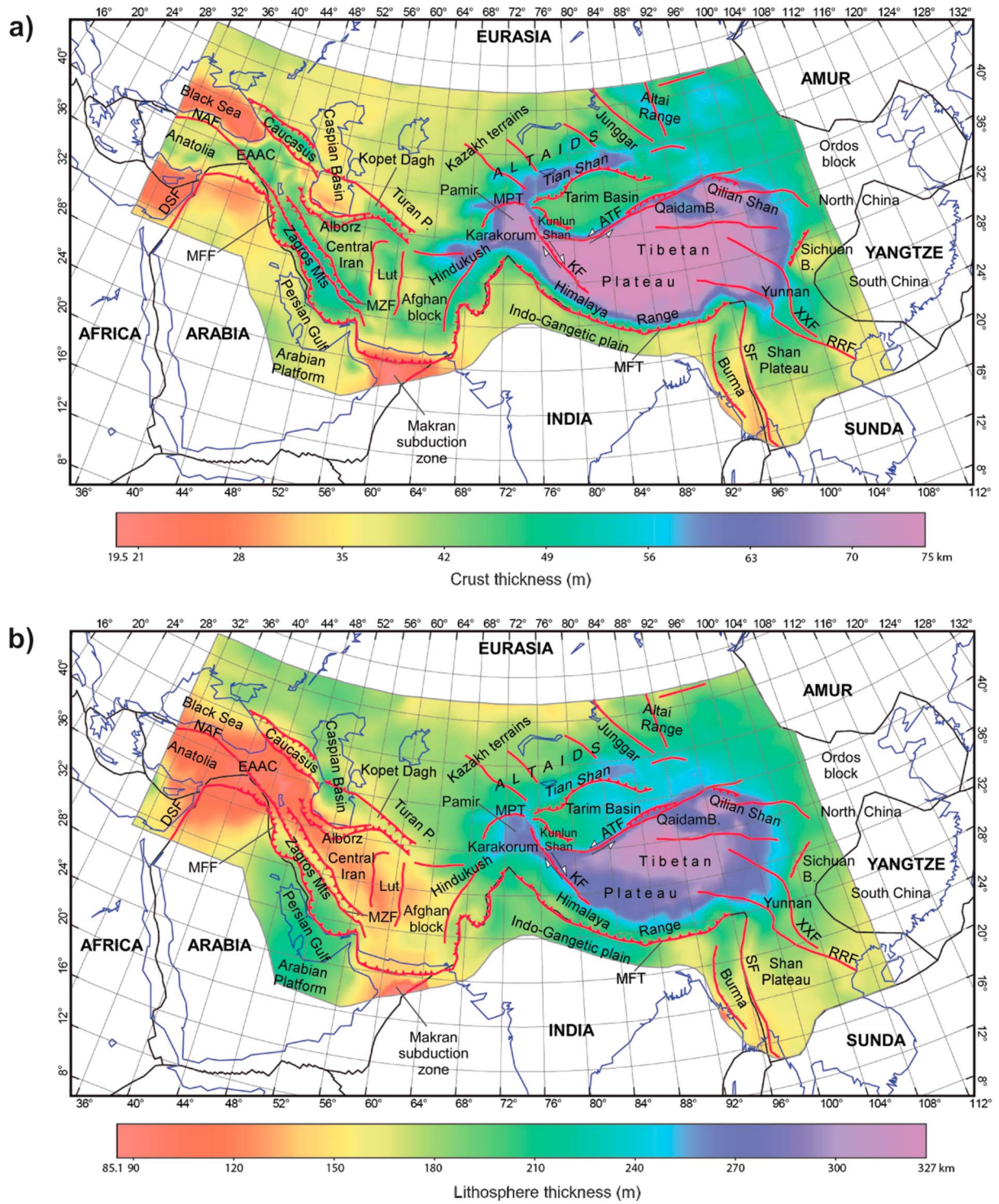

Figure 4. Input (a) crust and (b) lithosphere thickness of central Eurasia, derived from the combination of elevation, geoid anomaly and thermal analysis (by Robert et al., 2015). ATF: Altyn Tagh fault; DSF: Dead Sea fault; EAAC: Eastern Anatolia accretionary complex; KF: Karakorum fault; MFT: Main Frontal thrust; MFF: Mountain Front Flexure; MPT: Main Pamir thrust; MZF: Main Zagros fault; NAF: North Anatolia fault; RRF: Red River fault; SF: Sagaing fault; XXF: Xiangshuihe-Xiaojiang fault.

Table 1
Euler Poles From Liu and Bird (2008) of the Five Tectonic Plates in the Central Eurasia Region Referred to the Fixed Eurasia Plate

Plate name	N-Lat (deg)	E-Lon (deg)	Rotation rate (deg/Myr)
Amur	58.8	157.5	0.034
Arabia	26.22	22.87	0.427
India	28.56	11.62	0.357
Yangzte	61.21	142.00	0.206
Sunda	26.0	279.6	0.128

velocities and stress orientations with the available GPS and stress data. The northern boundary is part of stable Eurasia, and its velocity is set to zero. The Arabia plate, at the south-west corner of the study region, is moving NNE-ward, pushing against Eurasia at a rate 10–30 mm/yr increasing toward the south-east, consistent with the rate of 18–25 mm/yr inferred by geodetic measurements (Vernant et al., 2004). The India plate is advancing roughly NE-ward (~45 mm/yr), twice as fast as the Arabia plate, and with an increasing azimuth toward the east. The eastern segment of the southern boundary lies on the Sunda plate, and it is moving eastward with respect to the Eurasia plate with velocities $\leq$10 mm/yr. The velocities along the eastern boundary of the model domain are those resulting from the movements of the Amur and Yangtze plates. The Yangtze and Amur plates are moving ESE-ward with velocities between 11 and 16 mm/yr and ~2 mm/yr, respectively. The western boundary south of the North Anatolia fault (NAF) is set to free, allowing the westward escape of the Anatolia peninsula.

4.3. Model Constraints

The SHELLS program predicts time-average horizontal velocities, anelastic strain rates, stress directions, tectonic regimes, and fault slip rates and rakes. To evaluate the quality of the modeling results, we compare the model predictions with the surface velocities from geodetic studies, earthquake strain distribution, horizontal stress directions, tectonic regime, and fault slip rate measurements.

Figure 2a shows the velocity field derived from GPS observations in central Eurasia. In the western sector, GPS data (Mousavi et al., 2013; Reilinger et al., 2006; Tavakoli et al., 2008; Walpersdorf et al., 2014; Zarifi et al., 2013) reveal a rapid (~20–30 mm/yr) counterclockwise motion of the Arabia peninsula, Iran, and Anatolia/Aegean regions. In the Himalaya-Tibet region the GPS velocities (Bettinelli et al., 2006; Calais et al., 2006; Gan et al., 2007; Jade et al., 2004; Mohadjer et al., 2010; Socquet et al., 2006) show that part of the NNE-ward penetration of India into Tibet is absorbed by eastward and southward transfer of material around the eastern end of the Himalaya (e.g., Gan et al., 2007; Holt et al., 2000; Wang et al., 2001; Zhang et al., 2004). The eastward and southward transfer generates a glacier-like flow zone that turns ~180° clockwise around the eastern Himalaya syntaxis, and it ends in the Shan plateau with a fan-like front. Velocity vectors show that the average convergence rate is different between Arabia-Eurasia and India-Eurasia collision zones. In the former case, the current convergence rate is approximately 18–25 mm/yr in NNE direction (Sella, Dixon, & Mao, 2002; Vernant et al., 2004), with the deformation mostly accommodated along the main mountain ranges, the Alborz in the north, and the Zagros in the south. Only 10% of the overall Arabia-Eurasia convergence rate is absorbed along N-S trending strike-slip faults, which cross the Iranian plateau (Hatzfeld & Molnar, 2010; Vernant et al., 2004). The convergence rate between the Eurasia and India plates is higher, approximately 40–50 mm/yr, and directed NNE (Bettinelli et al., 2006; Calais et al., 2006), and only ~20 mm/yr is absorbed in the Himalayan front. The rest of the deformation is propagated northward, producing crustal thickening and continuous mountain building. Finally, the Makran subduction zone accommodates 19 ± 2 mm/yr and transmits 6 ± 2 mm/yr to the Kopet-Dagh (Vernant et al., 2004).

Earthquake depths provide valuable information about the style of local deformation and the brittle strength of the lithosphere. The distribution of seismicity (Figure 2b) reveals that both Arabia-Eurasia and India-Eurasia collision zones are the loci of numerous deadly earthquakes (i.e., Tabriz twin earthquakes, Iran, 11 August 2012, *M*6.3 and *M*6.4; Sichuan earthquake, eastern China, 12 May 2008, *M*8; Gorkha earthquake, Nepal, *M*7.9, 25 April 2015; and Kodari earthquake, Nepal, *M*7.3, 12 May 2015). In the Arabia-Eurasia collision zone the seismicity is mostly concentrated in the belts surrounding the more stable, relatively aseismic, central Iran, Lut, and South Caspian blocks. The majority of the moderate-sized (magnitude M_w ~ 5–6) earthquakes occur in the lower sedimentary cover, between 5 and 10 km depth (Adams et al., 2009; Maggi et al., 2000; Nissen et al., 2011; Talebian & Jackson, 2004; Tatar, Hatzfeld, & Ghafory-Ashtiany, 2004). Nissen et al. (2011) propose that since *M* ~ 5 events typically affect either the sedimentary cover or the basement but not both, the salt deposits act as an effective barrier to rupture propagation at the base of the sedimentary succession. Focal mechanism solutions and other stress indicators show compressional regimes along the Zagros front (Figure 2c), with a NNE-SSW direction of compression, oblique to the strike of the range. The tectonic regime is also compressional further north, in the Kopet Dagh, Alborz and Caucasus ranges. Strike-slip regimes are

Table 2
Model Parameters

Parameters	Values	Units
Crustal density at STP	2,825	kg m^{-3}
Lithospheric mantle density at STP	3,343	kg m^{-3}
Asthenosphere density at STP	3,200	kg m^{-3}
Water density	1,031	kg m^{-3}
Surface temperature	15	°C
Thermal conductivity, crust/mantle	2.7/3.2	W K^{-1} * m^{-1}
Volumetric thermal expansion coefficient, crust/mantle	$0/3.5 \cdot 10^{-5}$	K^{-1}
Radioactive heat production, crust/mantle	$0.5 \cdot 10^{-6}/0$	W m^{-3}
Temperature at LAB	1,300	°C

Note. STP = standard temperature and pressure, at 20°C and 1 bar.

present, especially in NW Iran and around the Lut block. Extension in the N-S direction characterizes the northern boundary of the South Caspian block, due to subduction since ~5.5 Ma (Hollingsworth et al., 2008; Priestley, Baker, & Jackson, 1994). In the India-Eurasia collision zone seismicity is significant and higher than in the Arabia-Eurasia collision zone, with large-magnitude earthquakes ($M_w \geq 8$). A Benioff surface can be distinguished in the Burma region, shallow dipping eastward with earthquakes at depths less than 200 km (Huang & Zhao, 2006; Li et al., 2008). Seismic tomography images show that the slab is confined to the upper mantle with a dip angle of ~60°, sinking in the transition zone at southern latitudes (Li et al., 2008). The images show also low-velocity zones beneath the Tengchong volcanic complex (located at 25°N, 98°E), confined at depths of ~150 km, and beneath the Red River Fault (continuing into depths greater than 200 km). These anomalies seem to be respectively related to the eastward subduction beneath the Burma region and to upper mantle processes occurring beneath the South China Sea (Li et al., 2008). To the west, large to moderate-sized earthquakes occur at depths of 100 km or more beneath the western Himalayan syntaxis, Hindukush, and Kunlun Shan. Fault plane solutions and tomography images show a Benioff surface steeply dipping down to 250 km depth (Chen & Yang, 2004; Negredo et al., 2007). Stress data show a NS to NNE-SSW trending compressional regime in front of the Himalayan range, in the Qilian Shan, in the eastern Tian Shan, and in the Altai range and a N-S or NNW-SSE compression in the central and western Tian Shan and Pamir regions (Figure 2c). Extensional and strike-slip features are observed throughout the Tibetan Plateau. Extension and strike-slip mechanisms characterize also the region around the eastern Himalaya syntaxis, to the west of the rigid Sichuan Basin, with a change from E-W to N-S direction of extension toward the east. Finally, the south-eastern portion of the central Eurasia region is characterized by joint strike-slip and compressional tectonics in the Burma region, Yunnan, and Shan plateau.

5. Results

The crustal and lithospheric mantle structure proposed by Robert et al. (2015) allows calculating the lateral variations of the vertically averaged strength and viscosity of the lithosphere over the study region. The thermal and rheological parameters used in these calculations are summarized in Tables 2 and 3, and we have run several models using a range of rheological parameter values from previous neotectonic studies (e.g., Barba et al., 2010; Bird & Kong, 1994; Burbidge, 2004; Jiménez-Munt & Sabadini, 2002; Negredo et al., 2002, 2004; Petit & Fournier, 2005; Vergnolle et al., 2007). We found good results with a fault friction coefficient of $\mu_f = 0.1$,

Table 3
Fault and Rheological Parameters

Parameter	Tested range	Average rheology (Figure 5)	Soft rheology (Figure 6)
Continuum friction	0.85	0.85	0.85
Fault friction	0.01/0.85	0.10	0.10
ACREEP crust (Pa $s^{-1/n}$)	$2.11 \cdot 10^6/2.3 \cdot 10^9$	$2.3 \cdot 10^9$	$2.3 \cdot 10^9$
ACREEP mantle (Pa $s^{-1/n}$)	$1.00 \cdot 10^4/1.4 \cdot 10^5$	$9.5 \cdot 10^4$	$1.00 \cdot 10^4$
BCREEP crust (K)	4,000/8,625	4,000	4,000
BCREEP mantle (K)	10,000/18,314	18,314	16,000
CCREEP crust (K m^{-1})	0	0	0
CCREEP mantle (K m^{-1})	0.0171	0.0171	0.0171
DCREEP (Pa)	$5 \cdot 10^8$	$5 \cdot 10^8$	$5 \cdot 10^8$
ECREEP =1/*n*	0.3333	0.3333	0.3333
TAUMAX (N/m)	$1.5 \cdot 10^{12}/4.5 \cdot 10^{13}$	$6 \cdot 10^{12}$	$6 \cdot 10^{12}$

Note. Equivalences with classical power law creep parameters are ACREEP = 1/a; BCREEP = Q/nR; ECREEP = 1/n; CCREEP is the derivative of BCREEP with respect to depth, CCREEP = $\rho g V_a/nR$); with a the preexponential creep parameter, Q the activation energy, V_a the activation volume, n the power law exponent, ρ the density, g the gravitational acceleration, and R the gas constant. DCREEP is the maximum shear strength. TAUMAX is the limit of vertical integral of shear traction of the subductions faults, MFF and MFT. See the text and Bird et al. (2008) for all the formulation.

similar to the values proposed in different neotectonic models: 0.1 in the Australian plate (Burbidge, 2004), 0.03 in the Caribbean plate (Negredo et al., 2004), 0.1 in southern Africa (Bird et al., 2006), 0.02 in the Arabia-Eurasia collision zone (Vernant & Chery, 2006), and 0.1 in a global model (Bird et al., 2008). The results presented in this section correspond to an average rheology (Model 1 in Table 3), and the influence of changing the rheological parameters is discussed in the next section. The goodness of the model is evaluated by comparing its predictions (long-term-average horizontal velocities, strain rates, horizontal stress directions, tectonic regime, and fault slip rates), with available data on seismic deformation, stress directions, and GPS velocities.

Figure 5a shows the vertically integrated lithospheric viscosity in the region, with values ranging from 10^{26} to 10^{30} Pa s m. Considering an average lithospheric thickness of ~10^5 m, the resulting mean viscosities are between 10^{21} and 10^{25} Pa s. Several rigid blocks characterized by higher viscosity values (Arabian peninsula, Caspian basin, Iranian plateau, Turan platform, Kazakh terranes, Indo-Gangetic plain, Altaids, Tarim and Sichuan basins, and Burma and Shan plateau regions) surround a rheologically weaker region, which includes most of the Alpine-Himalayan orogen (Anatolia, NW Iran, S-Caucasus, Pamir, Karakorum and Himalaya ranges, Tibetan Plateau, Qilian Shan, and South Burma region). In these softer areas the integrated viscosity ranges between $6.3 \cdot 10^{26}$ and $2.5 \cdot 10^{28}$ Pa s m, resulting in viscosity values of 10^{22} to 10^{23} Pa s.

Figure 5b shows the deformation pattern as the logarithm of the greatest principal strain rate and the horizontal velocity field. The stiffer blocks in the Arabia-Eurasia collision region (Caucasus, Caspian Sea, and Arabian platform) behave rigidly with low strain rate values, the strain being accommodated in Anatolia, south of Caucasus, and to less extent, in the Zagros Mountains. The northern and south-eastern regions of the Afghan block show also large strain rate values. The deformation resulting from the India-Eurasia convergence is mostly accommodated in the Hindukush, Pamir and Karakorum, and in the southern Tibetan Plateau. The strain rate in these areas is 1 order of magnitude higher than in the distant ranges of Altaids and Qilian Shan. The rigid blocks of the Indo-Gangetic plain, Tarim, Qaidam and Sichuan basins, and the Shan Plateau show negligible strain rate.

The convergence between Arabia-India and Eurasia is partly absorbed by the prescribed faults as shown by the calculated slip rates (Figure 5a). In the Arabia-Eurasia collision region, a shortening velocity between 9 and 2 mm/yr (from SE to NW) is accommodated in the Main Frontal fault, in agreement with those predicted by GPS (Tatar et al., 2002; Vernant et al., 2004; Walpersdorf et al., 2006). The Makran subduction accommodates ~7 mm/yr, and the Alborz and Kopet Dagh ranges show values of ~9–12 mm/yr. The slip rates along the North Anatolia fault are between 5.5 and 7 mm/yr, which are significantly lower than those measured by GPS (~20 mm/yr; Reilinger et al., 2006). This is probably due to the dominant effects of mantle dynamics related to the southwestward relative tensions transmitted from the migrating Aegean arc, which follows the roll-back of the African slab. These complex tectonics are not considered in the model, resulting in lower E-W velocities of Anatolia (Figure 5b). In the India-Eurasia collision, the Main Frontal thrust absorbs between a third and a half of the deformation, with slip rates between 15 and 24 mm/yr resulting in faster shortening in the eastern sector, also calculated by other authors (Burgess et al., 2012; Kumar et al., 2006; Lavé & Avouac, 2000). The Altyn Tagh Fault is characterized by 3–3.5 mm/yr of left-lateral slip-rate, showing lower values when compared to the 5–6 mm/yr calculated from GPS measurements (Zhang et al., 2004) or the 9–14 mm/yr determined by geological constraints (Cowgill et al., 2009). The Sagaing Fault shows a dextral slip rate of 15–25 mm/yr, which is consistent with the 18 mm/yr obtained by geodetic measurements (Vigny et al., 2003) or elastic modeling (Socquet et al., 2006).

The predicted velocity vectors are compared with GPS-inferred velocities (Figure 5b). The model reproduces the regional trend of the observed velocities for the Arabia-Eurasia collision zone, with the westward extrusion of Anatolia and the spread deformation across the Zagros Mountains. The Iranian plateau and the Lut block show coherent motion with moderate internal deformation. Part of the deformation is accommodated further north, in the Alborz and Kopet Dagh, with slip rate values of 9–12 mm/yr. To the west of the Caspian basin, the modeled velocities indicate that deformation is completely absorbed across the north-western Zagros belt, which is in contrast with GPS data showing that most of the Arabia–Eurasia convergence, west of 50°E, takes place in the Caucasus and its southern basin (Vernant et al., 2004). In the India-Eurasia collision zone, the calculated velocity field represents a good approximation to the GPS velocity field in the Himalaya range and in the central to western Tibetan Plateau. Modeled velocities show a NE-ward decrease in their

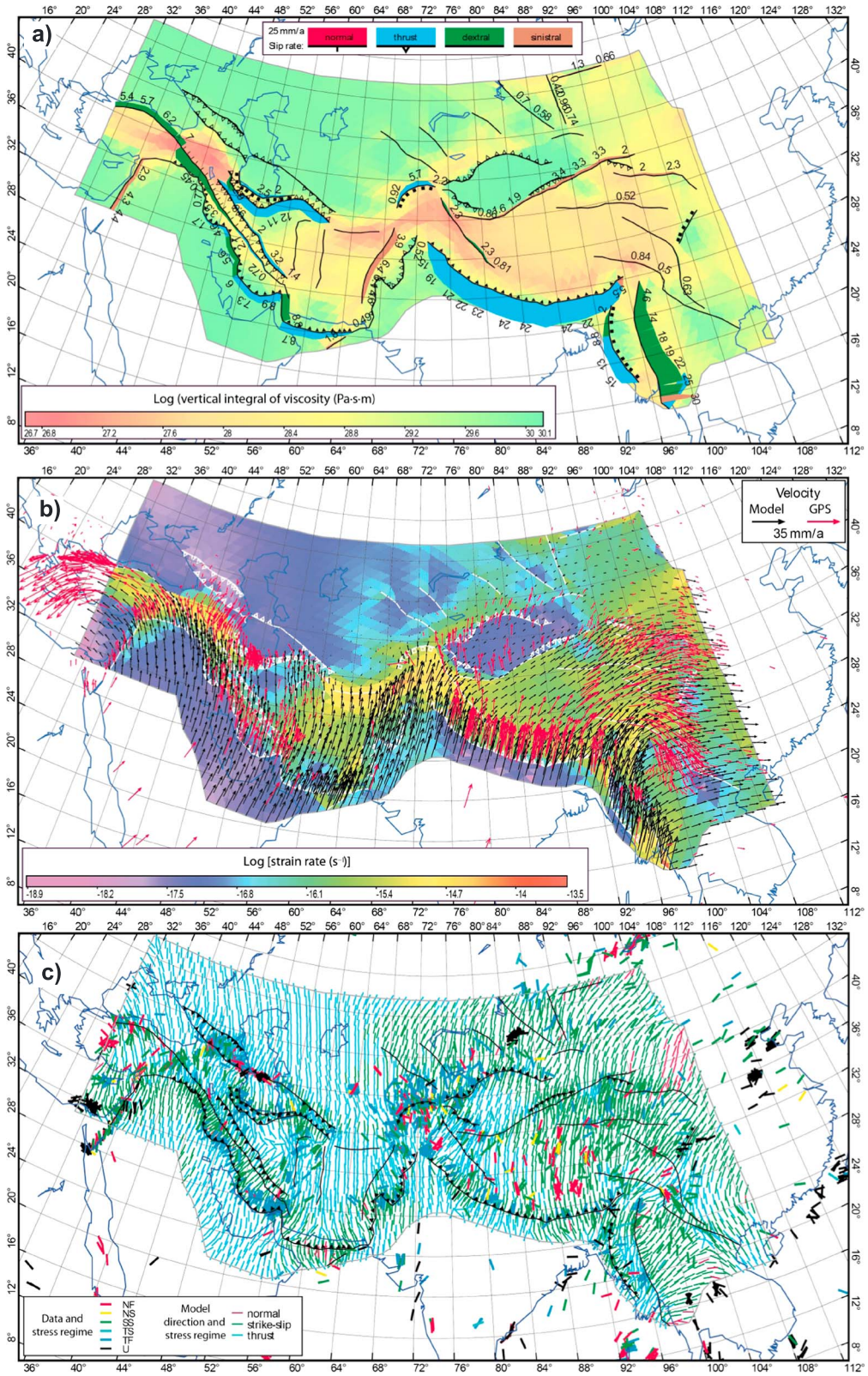

Figure 5. Reference model results assuming the lithosphere structure from Figure 4, modeling parameters in Tables 2 and 3, and fault friction coefficient $\mu_f = 0.1$. (a) Vertical integral of viscosity and slip rates on faults. (b) Magnitude of the greatest principal strain rate (background color), horizontal velocity field (black arrows), and measured GPS velocities (red arrows). Straining due to slip rates of fault elements is not included. (c) Directions of the most-compressive horizontal principal stresses (thinner lines), and stress data from WSM2008 (thicker lines, Heidbach et al., 2008). The color of the lines represents the tectonic regime.

magnitudes with minor changes in orientation, suggesting that a large amount of the north-eastward advancement of India is accommodated in the plateau, in agreement with geodetic observations. In NE-Tibet and in the Qilian Shan regions, the model velocities turn to the ENE, still fitting GPS data. However, the clockwise rotation of ~180° around the eastern Himalaya syntaxis is not reproduced. Predicted velocities from the model are only slightly deflected toward the south-east from 104°E, but in the Yunnan and across the Shan plateau they are directed eastward instead of southward. In the next section, we discuss different scenarious that better explain the velocity field in this region.

Figure 5c shows the calculated orientations of the most-compressive horizontal principal stress axis and the tectonic regime, compared to stress data coming from the World Stress Map WSM2008 (Figure 2c) (Heidbach et al., 2008). There is a general agreement between predicted stress orientations and the tectonic regime. Our results indicate thrusting with changing direction from N-S compression in north-western Iran and Caucasus to NNE-SSW in southern and eastern Iran. The tectonic regime in the Arabia/Eurasia collision zone is dominated by thrusting with some strike slip in the Zagros, Alborz, and Kopet Dagh ranges, in good agreement with the compiled data (Figure 2c). Major misfits occur in eastern Anatolia, where stress data indicate joint extensional and strike-slip deformation, which are not reproduced in the model. This extension is probably due to the southward retreat of the Hellenic subduction in the Aegean region, which is out of our model domain (Jiménez-Munt & Sabadini, 2002). In the India-Eurasia collision zone, the model stress field reproduces correctly the compressive regime in the Karakorum, Pamir, midwestern and western Himalaya, Kunlun Shan, and southern Tian Shan, as well as the joint strike-slip and compressive regime in the Qilian Shan, eastern Himalaya, and in the Shan plateau. In the northern Tian Shan and the Altai range the model predicts strike slip, though data indicate thrusting with some strike-slip. Moreover, the predicted stress orientations do not allow for extension throughout the Tibetan Plateau, nor between the eastern Tibetan syntaxis and the Sichuan Basin (Yunnan province), as indicated by focal mechanisms.

6. Discussion

The results presented in the previous section are subject to some modeling limitations. A first limitation associated with the SHELLS approach is that the lithospheric rheology is vertically averaged, and therefore, horizontal velocities (and strain rates) do not vary vertically or, in other words, the lithosphere behaves as a thin sheet. Though this approach has many computational advantages, the main drawback is that those observations that are compared to modeling results must be representative of the bulk lithosphere behavior. This is particularly critical for GPS velocities and stress orientations inferred from borehole data or shallow seismicity. A second limitation is that the rheological parameters, including the fault friction coefficient, are homogeneous over the whole model domain, whereas actually there may be different rheological regions. Bearing in mind these limitations we have explored the possible effects of varying the setup of the presented model to improve the results.

Recent integrated geophysical studies and tomographic models imply a thin mantle lithosphere beneath the north-eastern Tibetan Plateau to explain the low body- and surface-wave velocities, as well as the gravity, geoid, elevation, and surface heat flow observed in this region (Agius & Lebedev, 2013; Barron & Priestley, 2009; Ceylan et al., 2012; Jiménez-Munt et al., 2008; Kumar et al., 2006; Zhao et al., 2010). Results from the geophysical-petrological study carried out by Tunini et al. (2016) also confirm the presence of a shallower LAB in the north-eastern Tibetan Plateau, with the base of the lithosphere at ~120 km depth beneath the Bangong-Nujiang suture and northward up to latitude 36°N. The main effects of incorporating a reduction in lithospheric thickness of ~200 km beneath north-east Tibet are (i) the Moho temperature increases locally by ~200 °C with respect to the previous model; (ii) the vertically integrated lithosphere viscosity decreases by almost 1 order of magnitude, from $\sim 4 \cdot 10^{27}$ to $\sim 5 \cdot 10^{26}$ Pa s m; and (iii) the density of the lithospheric mantle in this region must be increased by ~25 kg/m^3 to keep the local isostatic condition. As a consequence, the NE-Tibet region shows an increase of ~16% in predicted strain rates and of ~40% in the predicted surface velocities, though normal faulting is not reproduced. In addition, the slip rates along the central and eastern segment of the MFT decrease by about 25%.

A weakness of the results shown in Figure 5 is the lack of E-W extension in the central Tibetan Plateau as inferred from the WSM2008 datafile, even when imposing a lithospheric thinning in its northern part. Strong rheologies can sustain large lateral GPE variations related to topographic contrasts, whereas weaker

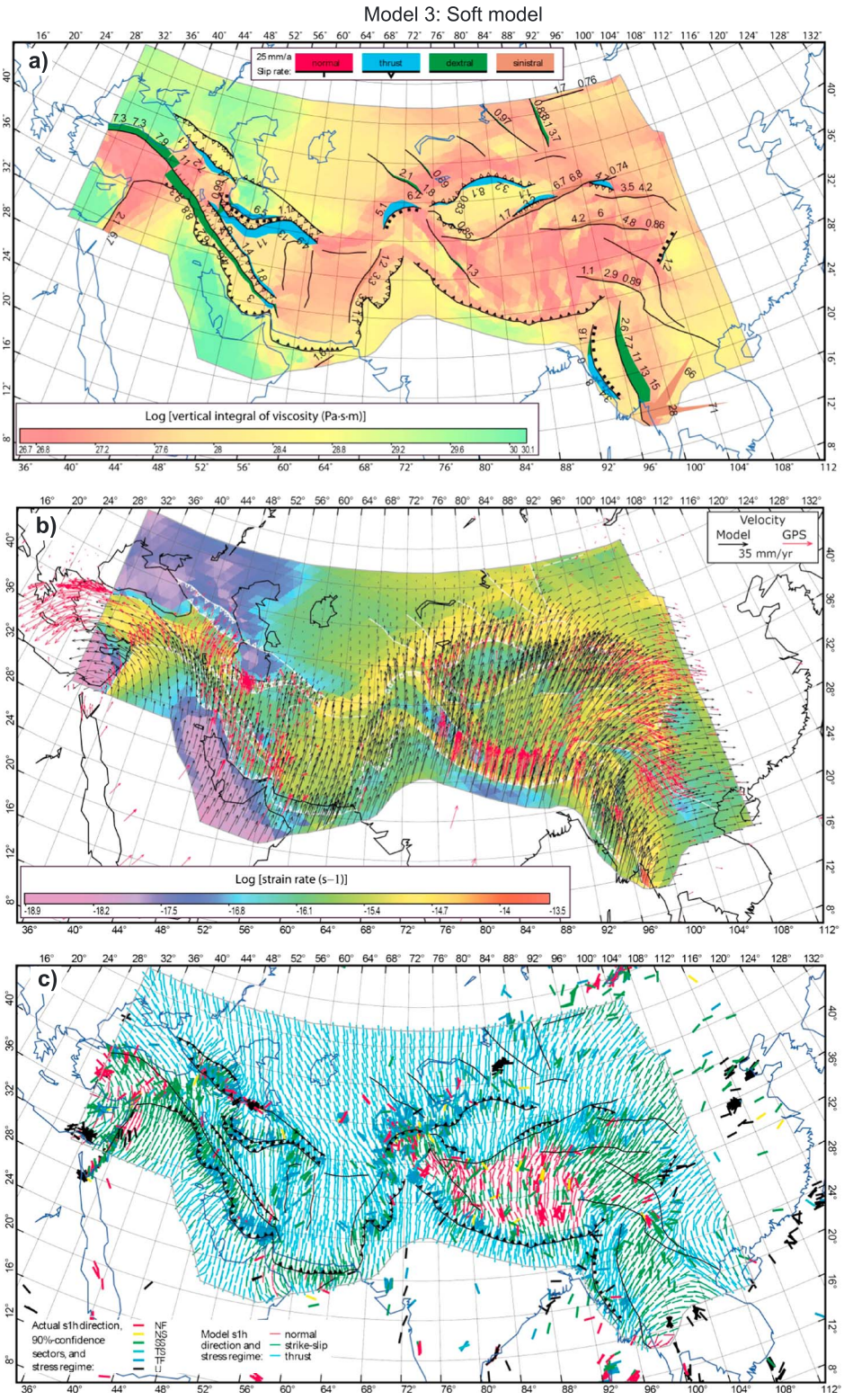

Figure 6. Model results assuming a softer rheology using the parameters described in Table 3. The lithosphere structure is the same than in Figure 4, and fault friction coefficient $\mu_f = 0.1$. (a) Vertical integral of viscosity and slip rates on faults. (b) Magnitude of the greatest principal strain rate (background color), horizontal velocity field (black arrows), and measured GPS velocities (red arrows). Straining due to slip rates of fault elements is not included. (c) Directions of the most-compressive horizontal principal stresses (thinner lines), and stress data from WSM2008 (thicker lines, Heidbach et al., 2008). The color of the lines represents the tectonic regime.

lithospheres respond to elevation variations by extension and topographic collapse in highlands. Following this argument, we considered a soft rheology (Table 3) that reduces the vertically integrated lithosphere viscosity by 1 order of magnitude in the deformed regions and by 2 orders of magnitude in the rigid blocks. The results are shown in Figure 6. The strain rate exceeds 10^{-16} s^{-1} in most of the study region, in contrast to the reference model in which such high strain rate values are restricted to the mountain ranges. Calculated long-term-average slip rates show negligible movement of the MFF in the Arabia-Eurasia collision zone, and the MFT in the India-Eurasia collision, because deformation is better transmitted to the interior of the continent, resulting in higher velocities in the northern areas (Turan Platform, Kazakh terranes, Tian Shan, and Altai range). This soft rheology model results in higher slip rate values in the Altyn Tagh Fault (5–7 mm/yr, in agreement with GPS measurements by Zhang et al., 2004), and lower in the Sagaing Fault (3–15 mm/yr). It also succeeds in reproducing the observed normal faulting in the central Tibetan Plateau. This model overestimates the observed GPS velocity values in central Iran (~16 mm/yr against ~12 mm/yr), Tarim Basin (~27 mm/yr against ~9.4 mm/yr), and Tian Shan (~18 mm/yr against ~15 mm/yr) and slightly underestimates the observations in north-western Iran (~27 mm/yr against ~33 mm/yr) and Caucasus (~8 mm/yr against 10 mm/yr). Figure 7 shows the fit of the GPS velocities for the reference model (Figure 5) and for the soft rheology model (Figure 6). The reference model provides better results in Anatolia, central Iran, Lut basin, and along the Himalaya range, eastern Tarim and Tian Shan, Altyn Tagh Fault, Quilian Shan, and Qaidam and Sichuan basins. The soft rheology model reproduces better the velocities in the Caucasus region, Alborz, western Tarim Basin, and Kunlun Shan. A soft Tibetan Plateau together with a stiff Tarim Basin (as proposed by Replumaz & Tapponnier, 2003) would better reproduce the measured slip rates in the ATF (5–6 mm/yr from Zhang et al., 2004, and 9–14 mm/yr from Cowgill et al., 2009) and the velocities in the Tian Shan (6–10 mm/yr from Gan et al., 2007). However, as mentioned before on the limitations of the numerical approach, SHELLS cannot incorporate lateral changes of rheological parameters.

Figure 8 compares the impact of considering models with softer rheological parameters, a thin lithosphere in NE Tibet, and the reference model, by scoring the predictions against GPS velocities and stress data using the root-mean-square (RMS) misfit. To have a full range of models, we have also varied the fault friction coefficient (μ_f) from 0.01 (weak faults) to 0.85 (same as in the continuum elements). To better illustrate the results, we plot separately the RMS misfit for the Arabia-Eurasia collision zone (from the western border of the study region to 62°E longitude) and for the India-Eurasia collision zone (from 66°E to the eastern border of the study region). The scores for the whole of central Asia (Figure 8a) show that considering a thinner lithosphere beneath NE Tibet has a reduced influence on the horizontal velocities and the mean stress azimuth. However, considering a softer rheology produces a better fit (lower RMS misfits) in the mean stress azimuth but a worse fit to the horizontal velocities. A remarkable result is that μ_f values in the range of 0.1–0.2 yield the best fit, except for the case of soft rheology, which shows lower mean stress azimuth errors when increasing μ_f.

In the Arabia-Eurasia collision zone (Figure 8b) a soft rheology produces a better fit to the horizontal velocities and stress directions, spreading the deformation to the north and causing higher velocities in Kopet Dagh, Alborz, and eastern Anatolia. The India-Eurasia collision zone (Figure 8c) shows remarkable better fits in both horizontal velocities and mean stress azimuth and is almost independent on the fault friction coefficient for values of $\mu_f > 0.2$. The thinning of the lithosphere in the NE Tibetan Plateau has no effect on the fit of the geodetic velocities, but it produces a slight improvement on the stress orientation. It must be noted that the degree of fitting with the selected observables (geodetic velocity and stress azimuth) is largely depending on the number and spatial distribution of these observations, and on its representability as plate kinematic variables. Then, in settings dominated by crust-mantle decoupling or local deformations, the quality of the model can decrease dramatically. This can be the case of the Caucasus in the Arabia-Eurasia collision region, and the Shan plateau in the eastern Himalaya syntaxis, where the major misfits are observed. Actually, removing the Caucasus results reduces the RMS misfit of geodetic velocities of the Arabia-Eurasia collision region from 9–10 mm/yr to 4 mm/yr (Figure 8b).

The rigid Afghan block occupies the region between the collisions of Arabia and India against Eurasia. The deformation of this intercollision zone is mainly related to the Makran subduction resulting in a dominant compressive tectonic regime over the whole region with N-S directed thrust faulting and northward horizontal velocities (Figure 5). Deformation is mainly localized in the northern border of this block (Herat Fault (HRF); Figure 3) with strain rates exceeding by 1 order of magnitude those calculated for the central part.

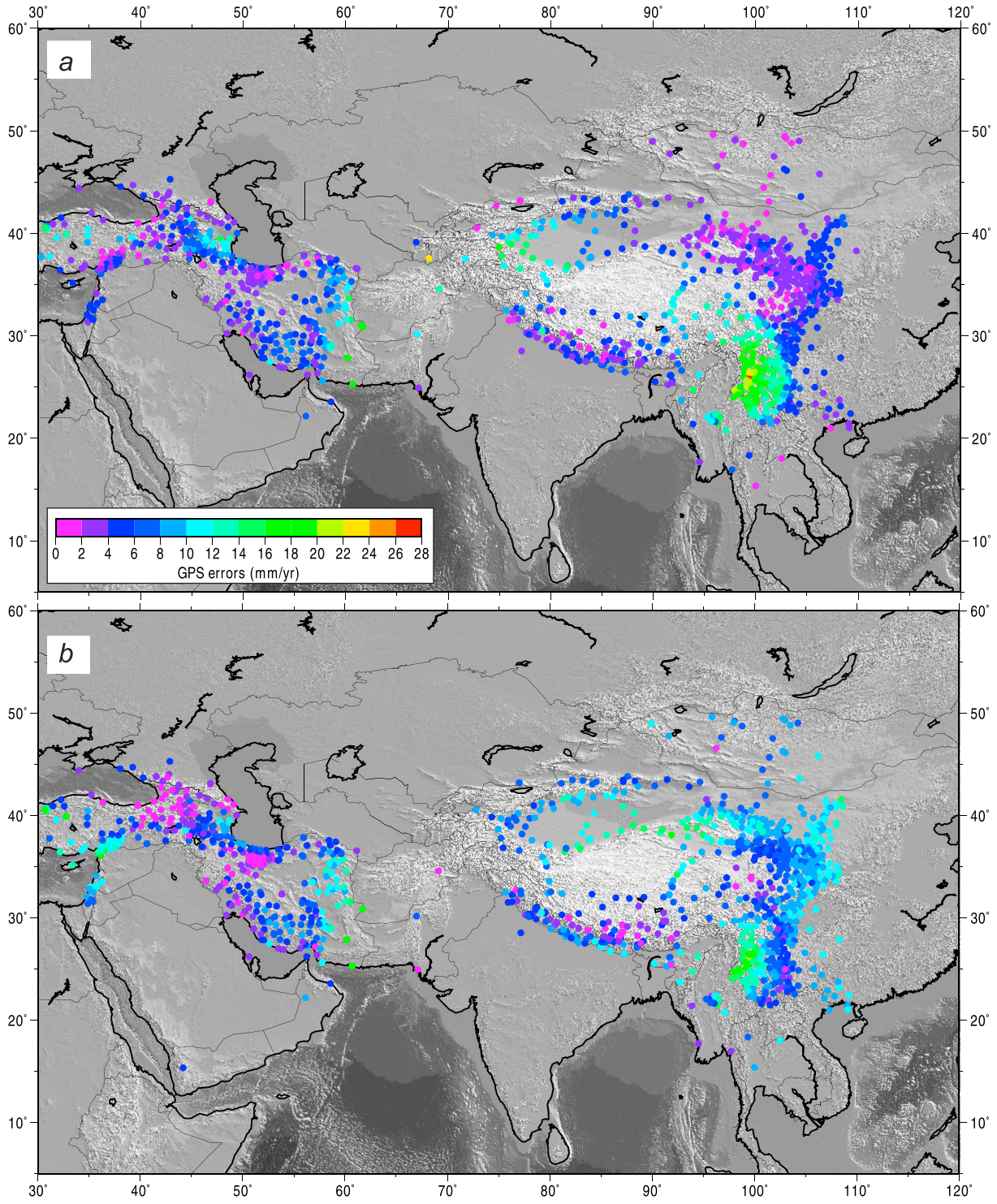

Figure 7. Misfits between the velocities from GPS observations and the velocities calculated from the model. (a) Reference model. (b) Soft-rheology model.

The northern convergence between the subducting Oman oceanic lithosphere and the Afghan block is accommodated by thrusting along the Makran trench with slip rates of up to 8.7 mm/yr. The relative movement of Arabia and India relative to the Afghan block is accommodated by right- and left-slip fault systems connecting the Makran front and the Main Zagros fault (MZF) and the MFT, respectively. Agard et al. (2011)

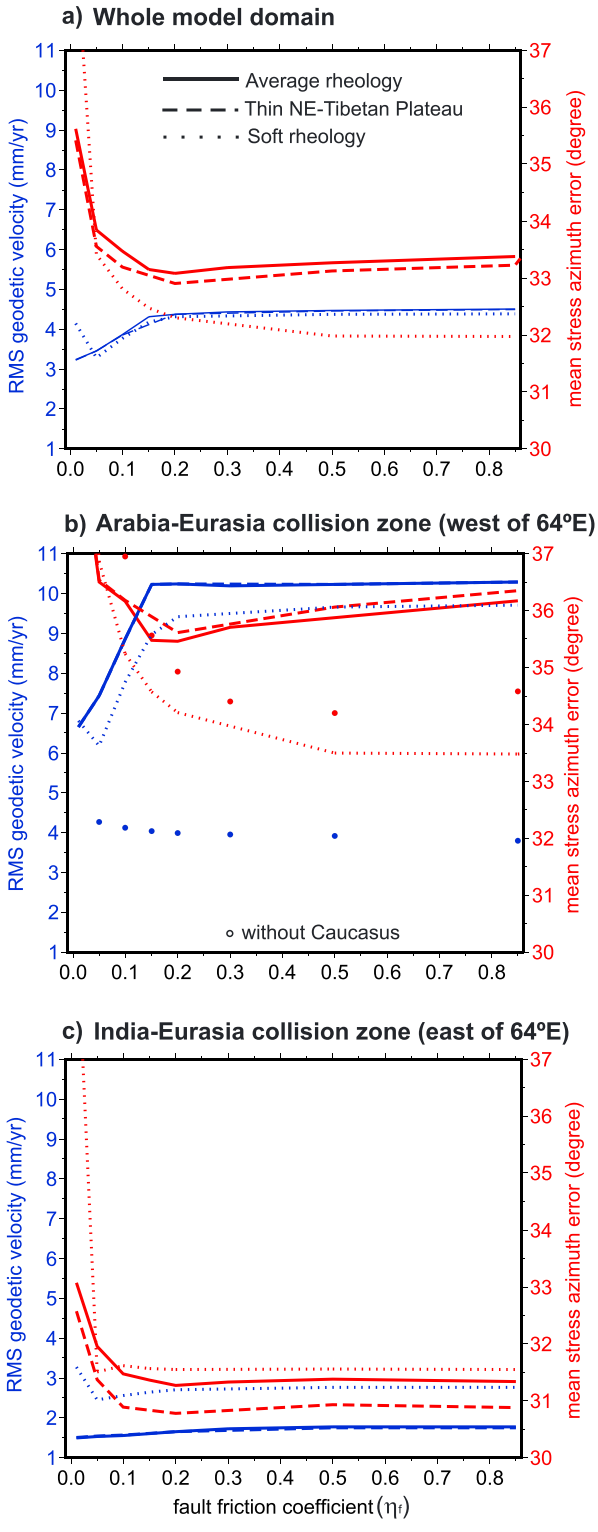

Figure 8. Model scores against geodetic velocities (left axis, in blue) and stress direction (right axis, in red) data for different fault friction coefficients ($0.01 < \mu_f < 0.85$) in the (a) whole region, (b) Arabia-Eurasia, and (c) India-Eurasia collision zones. The continuous lines for the reference model, the dashed lines considering a thinner lithosphere in the Tibetan Plateau, and the pointed lines a model with softer rheology. The dots in Figure 8b are results from the Arabia-Eurasia collision without the Caucasus zone.

suggested that the counterclockwise rotation and the westward escape of Anatolia are the indirect results of the collision between India and the Afghan block occurred around 5 Ma. This collisional event is thought to generate the change of the kinematic pattern on the Eurasian side of the Arabia-Eurasia collision from an eastward (toward Afghanistan) to westward (toward Anatolia) escape and also to play a role in the slow-down of convergence between Arabia and Eurasia (Austermann & Iaffaldano, 2013). Model results show slip rates up to 6.4 mm/yr along the eastern boundary of the Afghan block (Chaman Fault).

An outstanding characteristic of the measured GPS velocities is the abrupt change of ~180° in the velocity direction around the eastern Himalaya syntaxis, which is not reproduced by any of the presented models. Certainly, the model by Liu and Bird (2008) reproduced this sharp change of the velocity field by imposing the measured geodetic velocities, the fault slip rates, and the stress/strain rate directions in a purely kinematic approach, but without considering the acting forces and the lithosphere rheology. The complex subduction dynamics of SE Asia, with the interaction of the Eurasia, India, and Sunda plates, makes it difficult to reproduce the surface velocity field using a thin-shell approach. The same problem was pointed out by Vergnolle et al. (2007), who found that the predicted velocities show a systematic counterclockwise mismatch of 10°–15° compared to the geodetic observations in northern and eastern China.

Geodetic studies reveal that India-Sunda motion is partitioned between the right-lateral strike-slip Sagaing fault, slipping at a rate of 18 mm/yr, and the Arakan-Andaman trenches farther west, accommodating 20 mm/yr of oblique Indian convergence oriented ~30°N (Socquet et al., 2006). The Sagaing fault is linked to the Himalayan fault system by a compressional horsetail directed northward in the Himalayan syntaxis area, while it ends in an extensional horsetail toward the south in the Andaman pull-apart basin (Socquet et al., 2006). The Burma region is affected by moderate seismicity related to the Arakan-Andaman trenches and their southern propagation, the Sumatra trench, which form a huge arcuate subduction boundary between India, Australia, and Sunda plates. In this context, we have performed different models modifying the velocity conditions in the south-eastern boundary of central Eurasia by considering the possible effects of active subduction zones. In Figure 9a we show the boundary conditions that better reproduce the geodetic velocity in this region: the retreat of the Sumatra trench is dragging the Shan plateau southward, and the Arakan-Andaman trenches are a free boundary condition. With this configuration the calculated velocity field shows an ESE direction in the Sichuan basin turning into a SE to S direction in the Shan plateau due to the retreat of the Sumatra trench. However, the tight clockwise rotation in the velocity field, of 180° around the eastern Himalaya syntaxis, and the southward flow in the northern Shan plateau are not properly reproduced.

This problem could be associated with the relative values of the gravitational potential energy (GPE) and the lithospheric strength. The considered lithospheric structure and fault geometry result in a region too stiff to allow the southward movement of the Yunnan and Shan plateau. The most likely solutions would be to locally reduce the strength of the lithosphere, which could be done by changing fault dips to allow

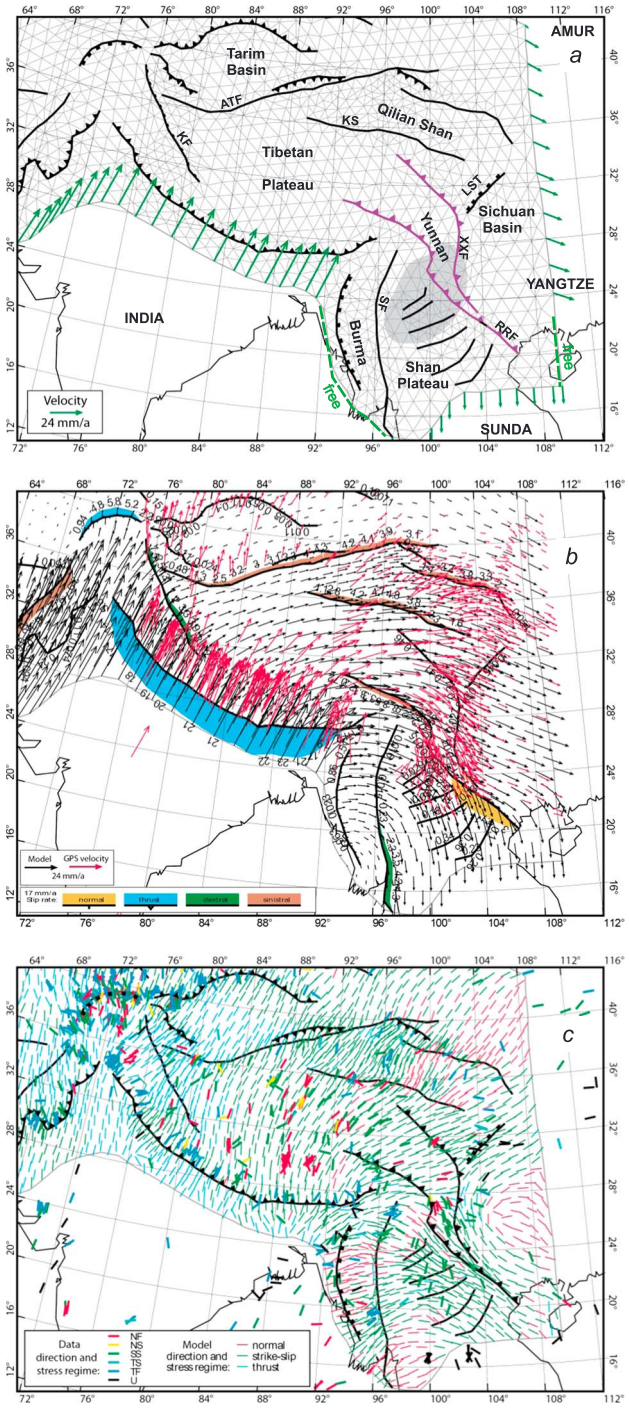

Figure 9. Modeling results considering the combined effects of southward Sumatra trench retreat, strike-slip faults in Shan Plateau and lithospheric mantle thinning in south Yunnan and north Shan plateau. Other model parameters are the same as in the reference model. (a) Mesh, faults, and boundary conditions. The purple faults denote dips of 45°, and the grey shaded area indicates lithospheric mantle thining. (b) Calculated horizontal velocities (black), GPS measurements (red), and fault slip rates. (c) Calculated most-compressive horizontal principal stress axes (thinner lines) and stress data from WSM2008 (thicker lines).

some dip-slip components, and/or adding more faults to the model. The Red River fault (RRF) and Xiangshuihe-Xiaojiang fault (XXF) are commonly considered pure strike-slip discontinuities (Replumaz et al., 2001; Taylor & Yin, 2009, and references therein). However, some authors have documented strike-perpendicular extension in the southern sector of the Red River (across the Ailao Shan; Harrison et al., 1996), with high-grade metamorphic rocks exposed along only one side of the fault. Therefore, *not* considering the entire RRF vertically dipping and admitting a dip change is a plausible approach. Thus, we changed the dips of the Red River and the Xianshuihe faults to 45° and we included additional faults in the Shan plateau, accordingly to Liu and Bird (2008) and Taylor and Yin (2009). The resulting deformation along the Red River fault is left slip in its NE segment and normal in its SE segment. This new configuration slightly favors the southward orientation of the velocities in Shan plateau.

South Yunnan and north Shan plateau are characterized by high surface heat flow (Tunini et al., 2016) and a low-velocity zone at 100 km depth (Huang & Zhao, 2006). This is compatible with a lithospheric mantle thinning, which would increase the Moho temperature and decrease the lithosphere strength. In Figure 9 we show the results of considering the retreat of the Sumatra trench, the new faults in the Shan plateau, and the lithospheric thinning beneath the southern Yunnan and northern Shan plateau (lithosphere thickness fixed to 80 km at the gray shaded area; Figure 9a). Consequently, the role of the GPE increases, making easier to transmit the retreat of the Sumatra trench to the north. As a result all of the Shan plateau is moving southward (Figure 9b), consistently with geodetic measurements. The calculated stress orientations (Figure 9c) show important differences. The stress regime changes from thrusting to normal faulting and strike slip in the Burma region when the NE directed push of the India plate is removed. Likewise, the stress regime changes from a dominant strike slip (Figure 5c) to normal faulting in the north and south-western Shan plateau (Figure 9c).

According to these results the clockwise rotation of the velocity field and the southward movement of the Shan plateau are due to a combination of several factors: (i) the southward retreat of the Sumatra trench, (ii) the existence of strike slip faults in the Shan plateau, and (iii) the lithospheric mantle thinning beneath south Yunnan and north Shan plateau. In this work we did not consider the asthenospheric flow, which could be an additional factor contributing to the southeast Asia extrusion as proposed by Sternai et al. (2016).

Figure 10 summarizes the results of this study, which offers a comprehensive model of the effects of the double collision of Arabia and India against Eurasia. Surface velocities from GPS observations are shown in red, depicting the well-known lateral escapes toward Anatolia and Eastern Asia. The Western escape toward Anatolia and Hellenides is mostly limited by the dextral North Anatolian fault, whereas the Eastern escape occurs southward of the sinistral Altyn Tagh fault. Calculated horizontal velocities from our model in the Arabia-India intercollision zone (Pakistan and Afghan block) are plotted in black, showing no major deflections related to the Arabia and India collisions. The larger velocity of Pakistan (India plate) with respect to the Afghan block (Arabia-Iran-Eurasia collision zone) is accommodated along the sinistral strike-slip Chaman fault system. The deformation in

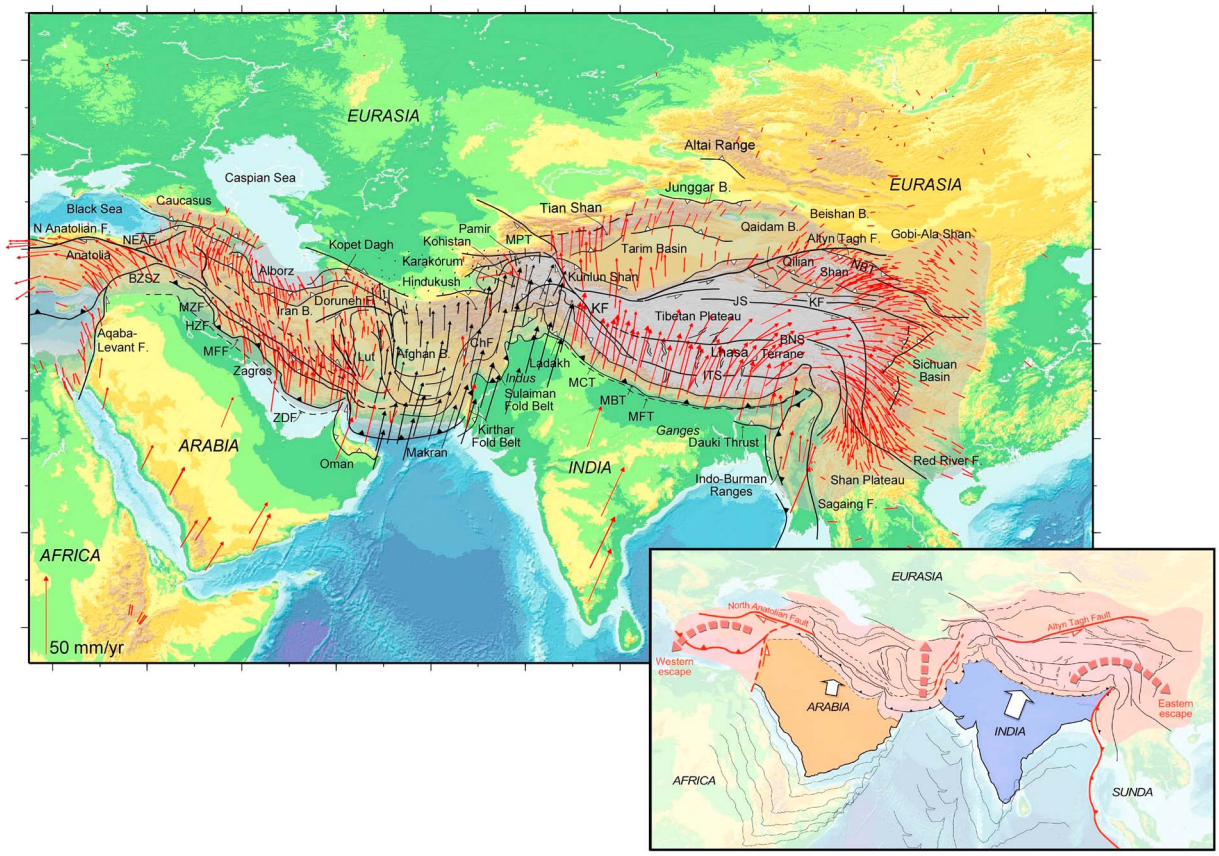

Figure 10. Tectonic map of the collision zone between Arabia and India plates with Eurasia plate, integrating GPS-derived velocities (red arrows), and horizontal velocities calculated from the model (black arrows). The sketch in the lower corner shows the inferred northward velocity direction of the intercollision zone (Pakistan and Afghan block), as well as the eastern and western escape tectonics produced by the westernmost Arabia and the easternmost India indenters. The thin black lines indicate the northward drift of Arabia and India plates based on Hatzfeld and Molnar (2010).

the Arabia-Eurasia collision zone propagates not beyond the northern boundary of the Afghan block coinciding with the Herat fault. Calculated velocities, strain rates, and stresses of the inter-collision zone have not been addressed in previous studies, so our results present new insights on the interaction between the two major Arabia and India continental collision systems.

7. Concluding Remarks

The thin viscous sheet approach used in this study reproduces the major features of the velocity, deformation pattern and stress fields in the central Eurasia region deformed by the collisions of Arabia and India plates with Eurasia plate. Besides the large scale, this study offers a coherent result in regions with little or no data coverage, as is the case of the Arabia-India intercollision zone, including the Afghan block and the western Himalaya syntaxis (Figure 8). From the presented results we conclude the following:

1. Average lithosphere viscosity shows large lateral variations between 10^{21} and 10^{25} Pa s in the central Eurasia region, related to both lithospheric mantle thicknesses and deformation rates and the amalgamation of rigid blocks surrounded by softer and more deformable tectonic domains.
2. Higher strain rates between 5.10^{-15} and 5.10^{-14} s^{-1} define the ~1,300 km wide Arabia-Eurasia and ~1,600 km wide India-Eurasia collision belts with the higher fault slip rates concentrated along the frontal thrusts of the Himalaya and Zagros in agreement with observed data. Maximum slip rates of 7.3, 8.7, and 24 mm/yr are predicted along the fronts of the Zagros, Makran, and Himalaya fold belts, respectively, by the preferred model.
3. The modeled velocity field shows two large west and east directed continental escape toroidal velocity fields along the NW corner of Zagros-Iran and the NE corner of Himalaya-Tibet orogenic systems fitting

GPS measurements. These modeled tectonic extrusions were the result of both strain rate and crustal and lithospheric thicknesses variations between the harder Eurasia plate and the softer amalgamated continental blocks that configured the southern margin of Eurasia before collision. The northern boundaries of western and eastern continental escapes are the North Anatolian fault and the Altyn Tagh fault, respectively.

4. The linking zone between the Arabia-Eurasia and India-Eurasia collisons across the Afghan block shows homogeneous north directed velocity field with no deflection caused by the Arabia or India continental indentors. Most deformation is concentrated along the sinistral strike-slip Chaman Fault with fault slip rates of 6.4 mm/yr.
5. N-S trending extensional normal faults in the Tibetan Plateau required using softer rheological parameters. A softer Tibetan Plateau is compatible with the proposed lithospheric thinning beneath it, inferred from the low seismic velocities observed in the upper mantle and from geophysical-petrological models.
6. Vertical strain partitioning related to crust-mantle decoupling, not included in these models, may be responsible for major misfits with geodetic measurements and stress azimuth data in the Caucasus Mountains and the eastern Tibet syntaxis.
7. The velocity field in the SE Tibetan Plateau can be explained by the combination of the southward Sumatra trench retreat, a lithospheric mantle thinning, and the presence of strike-slip faults.
8. The best fit requires fault friction coefficient values of $\mu_f \approx 0.1–0.2$. Model results show errors in GPS velocities of ~4 mm/yr and stress directions of ~33° in the whole model domain.

Acknowledgments
Funding was granted by the Spanish Government through the project MITE (CGL2014-59516-P) and ALPIMED (PIE-CSIC-201530E082). Figures in this paper have been produced using the open-source software GMT 4.0 (https://www.soest.hawaii.edu/gmt/) and FiniteMap (http://peterbird.name/).

References

Adamia, S., Zakariadze, G., Chkhotua, T., Sadradze, N., Tsereteli, N., Chabukiani, A., & Gventsadze, A. (2011). Geology of the Caucasus: A review. *Turkish Journal of Earth Sciences*, *20*, 489–544.

Adams, A., Brazier, R., Nyblade, A., Rodgers, A., & Al-Amri, A. (2009). Source parameters for moderate earthquakes in the Zagros mountains with implications for the depth extent of seismicity. *Bulletin of the Seismological Society of America*, *99*(3), 2044–2049. https://doi.org/10.1785/0120080314

Agard, P., Omrani, J., Jolivet, L., Whitechurch, H., Vrielynck, B., Spakman, W., … Wortel, R. (2011). Zagros orogeny: A subduction-dominated process. In O. Lacombe, B. Grasemann, & G. Simpson (Eds.), *Geodynamic evolution of the Zagros*, *Geological Magazine* (pp. 692–725). Cambridge: Cambridge University Press. http://doi.org/10.1017/S001675681100046X

Agius, M. R., & Lebedev, S. (2013). Tibetan and Indian lithospheres in the upper mantle beneath Tibet: Evidence from broadband surface-wave dispersion. *Geochemistry, Geophysics, Geosystems*, *14*(10), 4260–4281. https://doi.org/10.1002/ggge.20274

Amante, C., & Eakins, B.W. (2009). ETOPO1 arc-minute global relief model: Procedures, data sources and analysis, NOAA Technical Memorandum NESDIS NGDC-24, (19 pp.). Retrieved from http://www.ngdc.noaa.gov

Argus, D. F., Gordon, R. G., Heflin, M. B., Ma, C., Eanes, R. J., Willis, P., … Owen, S. E. (2010). The angular velocities of the plates and the velocity of Earth's centre from space geodesy. *Geophysical Journal International*, *180*(3), 913–960. https://doi.org/10.1111/j.1365-246X.2009.04463.x

Audet, P., & Bürgmann, R. (2011). Dominant role of tectonic inheritance in super-continent cycles. *Nature Geoscience*, *4*(3), 184–187. https://doi.org/10.1038/ngeo1080

Austermann, J., & Iaffaldano, G. (2013). The role of the Zagros orogeny in slowing down Arabia-Eurasia convergence since ~5 Ma. *Tectonics*, *32*(3), 351–363. https://doi.org/10.1002/tect.20027

Avagyan, A., Sosson, M., Karakhanian, A., Philip, H., Rebai, S., Rolland, Y., … Davtyan, V. (2010). Recent tectonic stress evolution in the Lesser Caucasus and adjacent regions. *Geological Society, London, Special Publications*, *340*(1), 393–408. https://doi.org/10.1144/SP340.17

Ballato, P., & Strecker, M. R. (2014). Assessing tectonic and climatic causal mechanisms in foreland-basin stratal architecture: Insights from the Alborz Mountains, northern Iran. *Earth Surface Processes and Landforms*, *39*(1), 110–125. https://doi.org/10.1002/esp.3480

Barba, S., Carafa, M. M. C., Mariucci, M. T., Montone, P., & Pierdominici, S. (2010). Present-day stress-field modelling of southern Italy constrained by stress and GPS data. *Tectonophysics*, *482*(1-4), 193–204. https://doi.org/10.1016/j.tecto.2009.10.017

Barron, J., & Priestley, K. (2009). Observations of frequency-dependent Sn propagation in northern Tibet. *Geophysical Journal International*, *179*, 474–488.

Berberian, M., & King, G. C. P. (1981). Towards a palegeography and tectonic evolution of Iran. *The Canadian Journal of Earth Sciences*, *18*(2).

Bettinelli, P., Avouac, J.-P., Flouzat, M., Jouanne, F., Bollinger, L., Willis, P., & Chitrakar, G. R. (2006). Plate motion of India and interseismic strain in the Nepal Himalayan from GPS and DORIS measurements. *Journal of Geodesy*, *80*(8-11), 567–589. https://doi.org/10.1007/s00190-006-0030-3

Bird, P. (1999). Thin-plate and thin-shell finite element programs for forward dynamic modeling of plate deformation and faulting. *Computational Geosciences*, *25*(4), 383–394. https://doi.org/10.1016/S0098-3004(98)00142-3

Bird, P. (2003). An updated digital model of plate boundaries, *Geochemistry, Geophysics, Geosystems*, *4*(3), 1027. https://doi.org/10.1029/2001GC000252

Bird, P., Ben-Avraham, Z., Schubert, G., Andreoli, M., & Viola, G. (2006). Patterns of stress and strain rate in southern Africa. *Journal of Geophysical Research*, *111*, B08402. https://doi.org/10.1029/2005JB003882

Bird, P., & Kong, X. (1994). Computer simulations of California tectonics confirm very low strength of major faults. *Geological Society of America Bulletin*, *106*(2), 159–174. https://doi.org/10.1130/0016-7606(1994)106%3C0159:CSOCTC%3E2.3.CO;2

Bird, P., Liu, Z., & Rucker, W. K. (2008). Stresses that drive the plates from below: Definitions, computational path, model optimization, and error analysis. *Journal of Geophysical Research*, *113*, B11406. https://doi.org/10.1029/2007JB005460

Bird, P., & Piper, K. (1980). Plane-stress finite-element models of tectonic flow in southern California. *Physics of the Earth and Planetary Interiors*, *21*(2-3), 158–175. https://doi.org/10.1016/0031-9201(80)90067-9

Bonini, M., Corti, G., Sokoutis, D., Vannucci, G., Gasperini, P., & Cloetingh, S. (2003). Insights from scaled analogue modelling into the seismotectonics of the Iranian region. *Tectonophysics*, *376*(3-4), 137–149. https://doi.org/10.1016/j.tecto.2003.07.002

Braun, I., & Kriegsmann, L. M. (2003). Proterozoic crustal evolution of southern most India and Sri Lanka. In M. Yoshida, B. F. Windley, & S. Dasgupta (Eds.), *Proterozoic East Gondwana: Supercontinent assembly and breakup*. *The Geological Society of London Special Publication* (Vol. 206, pp. 169–202). https://doi.org/10.1144/GSL.SP.2003.206.01.10

Burbidge, D. R. (2004). Thin plate neotectonic models of the Australian plate. *Journal of Geophysical Research*, *109*, B10405. https://doi.org/10.1029/2004JB003156

Burchfiel, B. C., Royden, L. H., van der Hilst, R. D., Hager, B. H., Chen, Z., King, R. W., … Kirby, E. (2008). A geological and geophysical context for theWenchuan earthquake of 12 May 2008, Sichuan, People's Republic of China. *GSA Today*, *18*(7), 4–11. https://doi.org/10.1130/GSATG18A.1

Burg, J.-P., Bernoulli, D., Smit, J., Dolati, A., & Bahroudi, A. (2008). A giant catastrophic mud-and-debris flow in the Miocene Makran. *Terra Nova*, *20*(3), 188–193. https://doi.org/10.1111/j.1365-3121.2008.00804.x

Burgess, W. P., Yin, A., Dubey, C. S., Shen, Z. K., & Kelty, T. K. (2012). Holocene shortening across the Main Frontal Thrust zone in the eastern Himalaya. *Earth and Planetary Science Letters*, *357*, 152–167.

Byrne, D. E., Sykes, L. R., & Davis, D. M. (1992). Great thrust earthquakes and aseismic slip along the plate boundary of the Makran subduction zone. *Journal of Geophysical Research*, *97*(B1), 449–478. https://doi.org/10.1029/91JB02165

Calais, E., Dong, L., Wang, M., Shen, Z., & Vergnolle, M. (2006). Continental deformation in Asia from a combined GPS solution. *Geophysical Research Letters*, *33*, L24319. https://doi.org/10.1029/2006GL028433

Calignano, E., Sokoutis, D., Willingshofer, E., Gueydan, F., & Cloetingh, S. (2015). Strain localization at the margins of strong lithospheric domains: Insights from analog models. *Tectonics*, *34*(3), 396–412. https://doi.org/10.1002/2014TC003756

Capitanio, F. A. (2014). The dynamics of extrusion tectonics: Insights from numerical modeling. *Tectonics*, *33*(12), 2361–2381. https://doi.org/10.1002/2014TC003688

Carafa, M. M. C., & Barba, S. (2011). Determining rheology from deformation data: The case of central Italy. *Tectonics*, *30*, TC2003. https://doi.org/10.1029/2010TC002680

Casciello, E., Vergés, J., Saura, E., Casini, G., Fernandez, M., Blanc, E., … Hunt, D. (2009). Fold patterns and multilayer rheology of the Lurestan Province, Zagros Simply Folded Belt (Iran). *Geological Society of London*, *166*, 1–13. https://doi.org/10.1144/0016-7649.2008-1138

Ceylan, S., Ni, J., Chen, J. Y., Zhang, Q., Tilmann, F., & Sandvol, E. (2012). Fragmented Indian plate and vertically coherent deformation beneath eastern Tibet. *Journal of Geophysical Research*, *117*, B11303. https://doi.org/10.1029/2012JB009210

Charvet, J., Shu, L. S., Laurent-Charvet, S., Wang, B., Michel, F., Dominique, C., … Koen, D. J. (2011). Paleozoic tectonic evolution of the Tianshan belt, NW China. *Science China: Earth Sciences*, *54*(2), 166–184. https://doi.org/10.1007/s11430-010-4138-1

Chen, W., & Yang, Z. (2004). Earthquakes beneath the Himalayas and Tibet: Evidence for strong lithospheric mantle. *Science*, *304*(5679), 1949–1952. https://doi.org/10.1126/science.1097324

Cook, K. L., & Royden, L. H. (2008). The role of crustal strength variations in shaping orogenic plateaus, with application to Tibet. *Journal of Geophysical Research*, *113*, B08407. https://doi.org/10.1029/2007JB005457

Cowgill, E., Gold, R. D., Xuanhua, C., & Xiao-Feng, W. (2009). Low Quaternary slip rate reconciles geodetic and geologic rates along the Altyn Tagh fault, northwestern Tibet. *Geology*, *37*(7), 647–650. https://doi.org/10.1130/G25623A.1

Cunha, T. A., Matias, L. M., Terrinha, P., Negredo, A. M., Rosas, F., Fernandes, M. S., & Pinheiro, L. M. (2012). Neotectonics of the SW Iberia margin, Gulf of Cadiz and Alboran Sea: A reassessment including recent structural, seismic and geodetic data. *Geophysical Journal International*, *188*(3), 850–872. https://doi.org/10.1111/j.1365-246X.2011.05328.x

DeMets, C., Gordon, R. G., & Argus, D. F. (2010). Geologically current plate motions. *Geophysical Journal International*, *181*(1), 1–80. https://doi.org/10.1111/j.1365-246X.2009.04491.x

DeMets, C., Gordon, R. G., Argus, D. F., & Stein, S. (1990). Current plate motions. *Geophysical Journal International*, *101*(425–478), 1990.

Egan, S. S., Mosar, J., Brunet, M.-F., & Kangarli, T. (2009). Subsidence and uplift mechanisms within the South Caspian Basin: Insights from the onshore and offshore Azerbaijan region. *Geological Society Special Publications*, *312*(1), 219–240. https://doi.org/10.1144/SP312.11

Emami, H., Vergés, J., Nalpas, T., Gillespie, P., Sharp, I., Karpuz, R., … Goodarzi, M. G. H. (2010). Structure of the Mountain Front Flexure along the Anaran anticline in the Pusht-e Kuh Arc (NW Zagros, Iran): Insights from sand box models. In P. Leturmy & C. Robin (Eds.), *Tectonic and stratigraphic evolution of Zagros and Makran during the Mesozoic-Cenozoic*, *Geological Society London Special Publication*, (Vol. 330, pp. 155–178).

Engdahl, E. R., van der Hilst, R., & Buland, R. P. (1998). Global teleseismic earthquake relocation with improved travel times and procedures for depth determination. *Bulletin of the Seismological Society of America*, *88*, 3295–3314.

England, P., & Housemann, G. (1989). Extension during continental convergence, with application to the Tibetan Plateau. *Journal of Geophysical Research*, *94*(B12), 17,561–17,579. https://doi.org/10.1029/JB094iB12p17561

England, P. C., & Molnar, P. (1997). The field of crustal velocity in Asia calculated from Quaternary rates of slip on faults. *Geophysical Journal International*, *130*(3), 551–582. https://doi.org/10.1111/j.1365-246X.1997.tb01853.x

Faccenna, C., Bellier, O., Martinod, J., Piromallo, C., & Regard, V. (2006). Slab detachment beneath eastern Anatolia: A possible cause for the formation of the North Anatolian fault. *Earth and Planetary Science Letters*, *242*(1-2), 85–97. https://doi.org/10.1016/j.epsl.2005.11.046

Flesch, L. M., Haines, A. J., & Holt, W. E. (2001). Dynamics of the India-Eurasia collision zone. *Journal of Geophysical Research*, *106*(B8), 16,435–16,460. https://doi.org/10.1029/2001JB000208

Gan, W., Zhang, P., Shen, Z.-K., Niu, Z., Wang, M., Wan, Y., … Cheng, J. (2007). Present-day crustal motion within the Tibetan Plateau inferred from GPS measurements. *Journal of Geophysical Research*, *112*, B08416. https://doi.org/10.1029/2005JB004120

Gao, C., & Ye, D. (1997). Petroleum geology of the Tarim basin, NW China: Recent advances. *Journal of Petroleum Geology*, *20*, 239–244.

Garcia-Castellanos, D., & Jiménez-Munt, I. (2015). Topographic evolution and climate aridification during continental collision: Insights from computer simulations. *PLoS One*, *10*(8), e0132252. https://doi.org/10.1371/journal.pone.0132252

Ghosh, A., Holt, W. E., Flesch, L. M., & Haines, A. J. (2006). Gravitational potential energy of the Tibetan Plateau and the forces driving the Indian Plate. *Geology*, *34*(5), 321–324. https://doi.org/10.1130/G22071.1

Guillot, S., Garzanti, E., Baratoux, D., Marquer, D., Maheo, G., & de Sigoyer, J. (2003). Reconstructing the total shortening history of the NW Himalaya. *Geochemistry, Geophysics, Geosystems*, *4*(7), 1064. https://doi.org/10.1029/2002GC000484

Harrison, T. M., Leloup, P. H., Ryerson, F. J., Tapponnier, P., Lacassin, R., & Wenji, C. (1996). Diachronous initiation of Transtension along the Ailao Shan-Red River Shear zone, Yunnan and Vietnam. In A. Yin & T. M. Harrison (Eds.), *The Tectonics of Asia, World and regional geology series* (pp. 208–226). Cambridge: Cambridge University Press.

Hatzfeld, D., & Molnar, P. (2010). Comparisons of the kinematics and deep structures of the Zagros and Himalaya and of the Iranian and Tibetan Plateaus and geodynamic implications. *Reviews of Geophysics*, *48*(2), RG2005. https://doi.org/10.1029/2009RG000304

Heidbach, O., Tingay, M., Barth, A., Reinecker, J., Kurfeß, D., & Müller, B. (2008). The 2008 release of the World Stress Map. Retrieved from http://www.world-stress-map.org, Helmholtz Centre Potsdam, Potsdam, Germany.

Hollingsworth, J., Jackson, J., Walker, R., & Nazari, H. (2008). Extrusion tectonics and subduction in the eastern South Caspian region since 10 Ma. *Geology*, *36*(10), 763–766. https://doi.org/10.1130/G25008A.1

Holt, W. E., Chamot-Rooke, N., Le Pichon, X., Haines, A. J., Shen-Tu, B., & Ren, J. (2000). Velocity field in Asia inferred from Quaternary fault slip rates and Global Positioning System observations. *Journal of Geophysical Research*, *105*(B8), 19,185–19,209. https://doi.org/10.1029/2000JB900045

Howe, T. C., & Bird, P. (2010). Exploratory models of long-term crustal flow and resulting seismicity across the Alpine-Aegean orogen. *Tectonics*, *29*(4), TC4023. https://doi.org/10.1029/2009TC002565

Huang, J., & Zhao, D. (2006). High-resolution mantle tomography of China and surrounding regions. *Journal of Geophysical Research*, *111*, B09305. https://doi.org/10.1029/2005JB004066

Jade, S., Bhatt, B. C., Yang, Z., Bendick, R., Gaur, V. K., Molnar, P., … Kumar, D. (2004). GPS measurements from the Ladakh Himalaya, India: Preliminary tests of plate-like or continuous deformation in Tibet. *Geological Society of America Bulletin*, *116*(11-12), 1385–1391. https://doi.org/10.1130/B25357.1

Jiménez-Munt, I., Fernandez, M., Saura, E., Vergés, J., & García-Castellanos, D. (2012). 3D lithospheric structure and regional/residual Bouguer anomalies from Arabia-Eurasia collision (Iran). *Geophysical Journal International*, *190*(3), 1311–1324. https://doi.org/10.1111/j.1365-246X.2012.05580.x

Jiménez-Munt, I., Fernandez, M., Torne, M., & Bird, P. (2001). The transition from linear to diffuse plate boundary in the Azores–Gibraltar region: Results from a thin-sheet model. *Earth and Planetary Science Letters*, *192*(2), 175–189. https://doi.org/10.1016/S0012-821X(01)00442-3

Jiménez-Munt, I., Fernandez, M., Vergés, J., & Platt, J. P. (2008). Lithosphere structure underneath the Tibetan Plateau inferred from elevation, gravity and geoid anomalies. *Earth and Planetary Science Letters*, *267*(1-2), 276–289. https://doi.org/10.1016/j.epsl.2007.11.045

Jiménez-Munt, I., Garcia-Castellanos, D., & Fernandez, M. (2005). Thin-sheet modelling of lithospheric deformation and surface mass transport. *Tectonophysics*, *407*(3-4), 239–255. https://doi.org/10.1016/j.tecto.2005.08.015

Jiménez-Munt, I., & Platt, J. P. (2006). Influence of mantle dynamics on the topographic evolution of the Tibetan Plateau: Results from numerical modeling. *Tectonics*, *25*(6), TC6002. https://doi.org/10.1029/2006TC001963

Jiménez-Munt, I., & Sabadini, R. (2002). The block-like behaviour of Anatolia envisaged in the modeled and geodetic strain rates. *Geophysical Research Letters*, *29*(20), 39-1–39-4, 1978. https://doi.org/10.129/2002GL015995

Jiménez-Munt, I., Sabadini, R., Gardi, A., & Bianco, G. (2003). Active deformation in the Mediterranean from Gibraltar to Anatolia inferred from numerical modeling and geodetic and seismological data. *Journal of Geophysical Research*, *108*(B1), ETG 2-1–ETG 2-24. https://doi.org/10.1029/2001JB001544

Keskin, M. (2003). Magma generation by slab steepening and breakoff beneath a subduction–accretion complex: An alternative model for collision-related volcanism in Eastern Anatolia, Turkey. *Geophysical Research Letters*, *30* (24), 8046. https://doi.org/10.1029/2003GL018019.

Khodaverdian, A., Zafarani, H., & Rahimian, M. (2015). Long term fault slip rates, distributed deformation rates and forecast of seismicity in the Iranian plateau. *Tectonics*, *34*(10), 2190–2220. https://doi.org/10.1002/2014TC003796

Kumar, P., Yuan, X., Kind, R., & Ni, J. (2006). Imaging the colliding India and Asian lithospheric plates beneath Tibet. *Journal of Geophysical Research*, *111*, B06308. https://doi.org/10.1029/2005JB003930

Kumar, P., Yuan, X., Kumar, M. R., Kind, R., Li, X., & Chadha, R. K. (2007). The rapid drift of the Indian tectonic plate. *Nature*, *449*(7164), 894–897. https://doi.org/10.1038/nature06214

Lavé, J., & Avouac, J. P. (2000). Active folding of fluvial terraces across the Siwaliks Hills, Himalayas of central Nepal. *Journal of Geophysical Research*, *105*(B3), 5735–5770. https://doi.org/10.1029/1999JB900292

Lechmann, S. M., Schmalholz, S. M., Hetenyi, G., May, D. A., & Kaus, B. J. P. (2014). Quantifying the impact of mechanical layering and underthrusting on the dynamics of the modern India-Asia collisional system with 3-D numerical models. *Journal of Geophysical Research: Solid Earth*, *119*, 616–644. https://doi.org/10.1002/2012JB009748

Li, C., van der Hilst, R., Meltzer, A., & Engdahl, E. (2008). Subduction of the Indian lithosphere beneath the Tibet Plateau and Burma. *Earth and Planetary Science Letters*, *274*(1-2), 157–168. https://doi.org/10.1016/j.epsl.2008.07.016

Li, Y., Wang, C., Ma, C., Xu, G., & Zhao, X. (2011). Balanced cross-section and crustal shortening analysis in the Tanggula-Tuotuohe Area, Northern Tibet. *Journal of Earth Science*, *22*(1), 1–10. https://doi.org/10.1007/s12583-011-0152-2

Liang, X., Sandvol, E., Chen, Y. J., Hearn, T., Ni, J., Klemperer, S., … Tilmann, F. (2012). A complex Tibetan upper mantle: A fragmented Indian slab and no south-verging subduction of Eurasian lithosphere. *Earth and Planetary Science Letters*, *333-334*, 101–111. https://doi.org/10.1016/j.epsl.2012.03.036

Liu, Z., & Bird, P. (2002). Finite elementmodeling of neotectonics in New Zealand. *Journal of Geophysical Research 107*(B12), ETG 1-1–ETG 1-18. https://doi.org/10.1029/2001JB001075

Liu, Z., & Bird, P. (2008). Kinematic modelling of neotectonics in the Persia-Tibet-Burma orogen. *Geophysical Journal International*, *172*(2), 779–797. https://doi.org/10.1111/j.1365-246X.2007.03640.x

Lu, S. N., Li, H. K., Zhang, C. L., & Niu, G. H. (2008). Geological and geochronological evidence for the Precambrian evolution of the Tarim craton and surrounding continental fragments. *Precambrian Research*, *160*(1-2), 94–107. https://doi.org/10.1016/j.precamres.2007.04.025

Maggi, A., Jackson, J. A., Priestley, K., & Baker, C. (2000). A re-assessment of focal depth distributions in southern Iran, the Tien Shan and northern India: Do earthquakes really occur in the continental mantle? *Geophysical Journal International*, *143*(3), 629–661. https://doi.org/10.1046/j.1365-246X.2000.00254.x

Marotta, A. M., Bayer, U., Scheck, M., & Thybo, H. (2001). The stress field bellow the NE German Basin: Effects induced by the Alpine collision. *Geophysical Journal International*, *144*(2), F8–F12. https://doi.org/10.1046/j.1365-246x.2001.00373.x

McQuarrie, N., & van Hinsbergen, D. J. J. (2013). Retro-deforming the Arabia-Eurasia collision zone: Age of collision versus magnitude of continental subduction. *Geology*, *41*(3), 315–318. https://doi.org/10.1130/G33591.1

Meert, J. G., Pandit, M. K., Pradhan, V. R., Banks, J., Sirianni, R., Stroud, M., … Gifford, J. (2010). Precambrian crustal evolution of Peninsular India: A 3.0 billion year odyssey. *Journal Asian Earth Science*, *39*(6), 483–515. https://doi.org/10.1016/j.jseaes.2010.04.026

Mohadjer, S., Bendick, R., Ischuk, A., Kuzikov, S., Kostuk, A., Saydullaev, U., … Molnar, P. (2010). Partitioning of India-Eurasia convergence in the Pamir-Hindu Kush from GPS measurements. *Geophysical Research Letters*, *37*(4), L04305. https://doi.org/10.1029/2009GL041737

Molinaro, M., Zeyen, H., & Laurencin, X. (2005). Lithospheric structure beneath the southeastern Zagros Mountains, Iran: Recent slab break-off? *Terra Nova*, *17*(1), 1–6. https://doi.org/10.1111/j.1365-3121.2004.00575.x

Morley, C. K., Kongwung, B., Julapour, A. A., Abdolghafourian, M., Hajian, M., Waples, D., … Kazemi, H. (2009). Structural development of a major late Cenozoic basin and transpressional belt in central Iran: The Central Basin in the Qom-Saveh area. *Geosphere*, *5*(4), 325–362. https://doi.org/10.1130/GES00223.1

Mosar, J., Kangarli, T., Bochud, M., Glasmacher, U. A., Rast, A., Brunet, M.-F., & Sosson, M. (2010). Cenozoic-recent tectonics and uplift in the Greater Caucasus: A perspective from Azerbaijan, Sedimentary Basin Tectonics from the Black Sea and Caucasus to the Arabian Plateform. *Geological Society, London, Special Publications*, *340*, 161–180.

Motavalli-Anbaran, S.-H., Zeyen, H., Brunet, M.-F., & Ardestani, V. E. (2011). Crustal and lithospheric structure of the Alborz Mountains, Iran, and surrounding areas from integrated geophysical modeling. *Tectonics*, *30*(5), TC5012. https://doi.org/10.1029/2011TC002934

Mousavi, S. M. (2016). Mapping seismic moment and b-value within the continental-collision orogenic-belt region of the Iranian Plateau. *Journal of Geodynamics*, *103*, 26–41.

Mousavi, Z., Walpersdorf, A., Walker, R. T., Tavakolim, F., Pathier, E., Nankali, H., … Djamour, Y., 2013. Global Positioning System constraints on the active tectonics of NE Iran and the South Caspian region. *Earth Planet Sci Lett*, *377–378*, 287–298. https://doi/org/10.1016/ j.epsl.2013.07.007

Mouthereau, F., Lacombe, O., & Vergés, J. (2012). Building the Zagros collisional orogen: Timing, strain distribution and the dynamics of Arabia/Eurasia plate convergence. *Tectonophysics*, *532-535*, 27–60. https://doi.org/10.1016/j.tecto.2012.01.022

Negredo, A. M., Bird, P., Sanz de Galdeano, C., & Buforn E. (2002). Neotectonic modeling of the Ibero-Maghrebian region. *Journal of Geophysical Research*, *107*(B11), ETG 10-1–ETG 10-15. https://doi.org/10.1029/2001JB000743

Negredo, A. M., Jiménez-Munt, I., & Villaseñor, A. (2004). Evidence for eastward mantle flow beneath the Caribbean plate from neotectonic modeling. *Geophysical Research Letters*, *31*(6), L06615. https://doi.org/10.1029/2003GL019315

Negredo, A. M., Replumaz, A., Villaseñor, A., & Guillot, S. (2007). Modeling the evolution of continental subduction processes in the Pamir–Hindu Kush region. *Earth and Planetary Science Letters*, *259*(1-2), 212–225. https://doi.org/10.1016/j.epsl.2007.04.043

Neres, M., Carafa, M. M. C., Fernandes, R. M. S., Matias, L., Duarte, J. C., Barba, S., & Terrinha, P. (2016). Lithospheric deformation in the Africa-Iberia plate boundary: Improved neotectonic modeling testing a basal-driven Alboran plate. *Journal of Geophysical Research: Solid Earth*, *121*(9), 6566–6596. https://doi.org/10.1002/2016JB013012

Nissen, E., Tatar, M., Jackson, J. A., & Allen, M. B. (2011). New views on earthquake faulting in the Zagros fold-and-thrust belt of Iran. *Geophysical Journal International*, *186*(3), 928–944. https://doi.org/10.1111/j.1365-246X.2011.05119.x

Petit, C., & Fournier, M. (2005). Present-day velocity and stress fields of the Amurian plate from thin-shell finite-element modelling. *Geophysical Journal International*, *160*(1), 357–369.

Priestley, K., Baker, C., & Jackson, J. (1994). Implications of earthquake focal mechanism data for the active tectonics of the south Caspian basin and surrounding regions. *Geophysical Journal International*, *118*(1), 111–141. https://doi.org/10.1111/j.1365-246X.1994.tb04679.x

Raeesi, M., Zarifi, Z., Nilfouroushan, F., Boroujeni, S. A., & Tiampo, K. (2016). Quantitative analysis of seismicity in Iran. *Pure and Applied Geophysics*, 1–41.

Reilinger, R., McClusky, S., Vernant, P., Lawrence, S., Ergintav, S., Cakmak, R., … Karam, G. (2006). GPS constraints on continental deformation in the Africa-Arabia-Eurasia continental collision zone and implications for the dynamics of plate interactions. *Journal of Geophysical Research*, *111*, B05411. https://doi.org/10.1029/2005JB004051

Replumaz, A., Lacassin, R., Tapponnier, P., & Leloup, P. H. (2001). Large river offsets and Plio-Quaternary destral slip rate on the Red River Fault (Yunnan, China). *Journal of Geophysical Research*, *106*(B1), 819–836. https://doi.org/10.1029/2000JB900135

Replumaz, A., & Tapponnier, P. (2003). Reconstruction of the deformed collision zone Between India and Asia by backward motion of lithospheric blocks. *Journal of Geophysical Research*, *108*(B6), 2285. https://doi.org/10.1029/2001JB000661

Rizaoglu, T., Parlak, O., Höck, V., Koller, F., Hames, W. E., & Billor, Z. (2009). Andean-type active margin formation in the eastern Taurides: Geochemical and geochronogical evidence from the baskil granitoid (Elazig, SE Turkey). *Tectonophysics*, *473*(1-2), 188–207. https://doi.org/10.1016/j.tecto.2008.08.011

Robert, A., Fernandez, M., Jiménez-Munt, I., & Vergés, J. (2015). Lithospheric structures in Central Eurasia derived from elevation, geoid anomaly and thermal analysis. *Journal of the Geological Society London, Special Publications*, *427*, 271–293. https://doi.org/10.1144/SP427.10

Robert, A., Letouzey, J., Müller, C., Kavoosi, M., Vergés, J., Sherkati, S., & Aghababei, A. (2014). Structural evolution of the Kopeh Dagh fold-and-thrust belt (NE Iran) and interactions with the South Caspian and Amu Darya basins. *Journal Marine and Petroleum Geology*, *57*, 68–87. https://doi.org/10.1016/j.marpetgeo.2014.05.002

Robert, X., van der Beek, P., Braun, J., Perry, C., Dubille, M., & Mugnier, J.-L. (2009). Assessing Quaternary reactivation of the Main Central thrust zone (central Nepal Himalaya): New thermochronologic data and numerical modelling. *Geology*, *37*(8), 731–734. https://doi.org/10.1130/G25736A.1

Robl, J., & Stüwe, K. (2005). Continental collision with finite indenter strength: 1. Concept and model formulation. *Tectonics*, *24*(4), TC4005. https://doi.org/10.1029/2004TC001727

Saura, E., Verges, J., Homke, S., Blanc, E., Serra-Kiel, J., Bernaola, G., … Hunt, D. W. (2011). Basin architecture and growth folding of the NW Zagros early foreland basin during the Late Cretaceous and early Tertiary. *Journal of the Geological Society*, *168*(1), 235–250. https://doi.org/10.1144/0016-76492010-092

Schmidt, J., Hacker, B. R., Ratschbacher, L., Stübner, K., Stearns, M., Kylander-Clark, A., … Minaev, V. (2011). Cenozoic deep crust in the Pamir. *Earth and Planetary Science Letters*, *312*(3-4), 411–421. https://doi.org/10.1016/j.epsl.2011.10.034

Schurr, B., Ratschbacher, L., Sippl, C., Gloaguen, R., Yuan, X., & Mechie, J. (2014). *Seismotectonics of the Pamir*. Washington, DC: American Geophysical Union.

Sella, G. F., Dixon, T. H., & Mao, A. (2002). REVEL: A model for recent plate velocities from space geodesy. *Journal of Geophysical Research*, *107*(B4), ETG 11-1–ETG 11-30. https://doi.org/10.1029/2000JB000033

Sengör, A. M. C., Altiner, D., Cin, A., Ustaomer, T., & Hsu, K. J. (1988). Origin and assembly of the Tethyside orogenic collage at the expense of Gondwana Land. *Geological Society of London, Special Publication*, *37*(1), 119–181. https://doi.org/10.1144/GSL.SP.1988.037.01.09

Sengör, A. M. C., Özeren, S., Genc, R., & Zor, E. (2003). East Anatolian high plateau as a mantle-supported, north-south shortened domal structure. *Geophysical Research Letters*, *30*(24), 8045. https://doi.org/10.1029/2003GL017858

Sepehr, M., & Cosgrove, J. W. (2004). Structural framework of the Zagros Fold-Thrust Belt Iran. *Marine and Petroleum Geology*, *21*(7), 829–843. https://doi.org/10.1016/j.marpetgeo.2003.07.006

Sherkati, S., Letouzey, Y., & Frizon de Lamotte, D. (2006). Central Zagros fold-thrust belt (Iran): New insights from seismic data, field observation and sandbox modeling. *Tectonics*, *25*(4), TC4007. https://doi.org/10.1029/2004TC001766

Smit, H. W., Cloetingh, S., Burov, E., Tesauro, M., Sokoutis, D., & Kaban, M. (2013). Interference of lithospheric folding in western Central Asia by simultaneous Indian and Arabian plate indentation. *Tectonophysics*, *602*, 176–193. https://doi.org/10.1016/j.tecto.2012.10.032

Sobouti, F., & Arkani-Hamed, J. (1996). Numerical modelling of the deformation of the Iranian Plateau. *Geophysical Journal International*, *126*(3), 805–818. https://doi.org/10.1111/j.1365-246X.1996.tb04704.x

Socquet, A., Vigny, C., Chamot-Rooke, N., Simons, W., Rangin, C., & Ambrosius, B. (2006). India and Sunda plates motion and deformation along their boundary in Myanmar determined by GPS. *Journal of Geophysical Research*, *111*, B05406. https://doi.org/10.1029/2005JB003877

Stern, R. J., & Johnson, P. (2010). Continental lithosphere of the Arabian plate: A geologic, petrologic, and geophysical synthesis. *Earth Science Reviews*, *101*(1-2), 29–67. https://doi.org/10.1016/j.earscirev.2010.01.002

Stern, R. J., & Johnson, P. R. (2008). Do variations in Arabian plate lithospheric structure control deformation in the Arabian–Eurasian convergence zone? Donald D. Harrington Symposium on the Geology of the Aegean. IOP Conf. Series. *Earth and Environmental Science*, *2*. https://doi.org/10.1088/1755-1307/2/1/012005

Sternai, P., Avouac, J. P., Jolivet, L., Faccenna, C., Gerya, T., Becker, T. W., & Menant, A. (2016). On the influence of the asthenospheric flow on the tectonics and topography at a collision-subduction transition zones: Comparison with the eastern Tibetan margin. *Journal of Geodynamics*, *100*, 184–197. https://doi.org/10.1016/j.jog.2016.02.009

Talebian, M., & Jackson, J. (2004). A reappraisal of earthquake focal mechanisms and active shortening in the Zagros mountains of Iran. *Geophysical Journal International*, *156*(3), 506–526. https://doi.org/10.1111/j.1365-246X.2004.02092.x

Tapponnier, P., Mattauer, M., Proust, J.-N., & Cassaigneau, C. (1981). Mesozoic ophiolites, sutures, and large-scale tectonic movements in Afghanistan. *Earth and Planetary Science Letters*, *52*(2), 355–371. https://doi.org/10.1016/0012-821X(81)90189-8

Tatar, M., Hatzfeld, D., & Ghafory-Ashtiany, M. (2004). Tectonics of the Central Zagros (Iran) deduced from microearthquake seismicity. *Geophysical Journal International*, *156*(2), 255–266. https://doi.org/10.1111/j.1365-246X.2003.02145.x

Tatar, M., Hatzfeld, D., Martinod, J., Walpersdorf, A., Ghafori-Ashtiany, M., & Chéry, J. (2002). The present-day deformation of the central Zagros from GPS measurements. *Geophysical Research Letters*, *29*(19), 33-1–33-4. https://doi.org/10.1029/2002GL015427

Tavakoli, F., Walpersdorf, A., Authemayou, C., Nankali, H. R., Hatzfeld, D., Tatar, M., … Cotte, N. (2008). Distribution of the right-lateral strike slip motion from the Main Recent Fault to the Kazerun Fault System (Zagros, Iran): Evidence from present-day GPS velocities. *Earth and Planetary Science Letters*, *275*(3-4), 342–347. https://doi.org/10.1016/j.epsl.2008.08.030

Taylor, M., & Yin, A. (2009). Active structures of the Himalayan-Tibetan orogen and their relationships to earthquake distribution, contemporary strain field, and Cenozoic volcanism. *Geosphere*, *5*(3), 199–214. https://doi.org/10.1130/GES00217.1

Tunini, L., Jiménez-Munt, I., Fernandez, M., Vergés, J., & Villaseñor, A. (2015). Lithospheric mantle heterogeneities below the Zagros Mountains and the Iranian Plateau: A petrological-geophysical study. *Geophysical Journal International*, *200*, 596–614.

Tunini, L., Jiménez-Munt, I., Fernandez, M., Vergés, J., Villaseñor, A., Melchiorre, A. M., & Afonso, J. C. (2016). Geophysical-petrological model of the crust and upper mantle in the India-Eurasia collision zone. *Tectonics*, *35*(7), 1642–1669. https://doi.org/10.1002/2016TC004161

van Hinsbergen, D. J. J., Kapp, P., Dupont-Nivet, G., Lippert, P. C., DeCelles, P. G., & Torsvik, T. H. (2011). Restoration of Cenozoic deformation in Asia and the size of Greater India. *Tectonics*, *30*(5), TC5003. https://doi.org/10.1029/2011TC002908

Vergés, J., Saura, E., Casciello, E., Fernandez, M., Villaseñor, A., Jiménez-Munt, I., & García-Castellanos, D. (2011). Crustal-scale cross-section across the NW Zagros Belt: Implications for the Arabian Margin reconstruction. In O. Lacombe, B. Grasemann, & G. Simpson (Eds.), *Geodynamic Evolution of the Zagros*, *Geological Magazine* (Vol. 148, pp. 739–761). Cambridge: Cambridge University Press. https://doi.org/10.1017/S0016756811000331

Vergnolle, M., Calais, E., & Dong, L. (2007). Dynamics of continental deformation in Asia. *Journal of Geophysical Research*, *112*, B11403. https://doi.org/10.1029/2006JB004807

Vernant, P., & Chery, J. (2006). Low fault friction in Iran implies localized deformation for the Arabia-Eurasia collision zone. *Earth and Planetary Science Letters*, *246*(3-4), 197–206. https://doi.org/10.1016/j.epsl.2006.04.021

Vernant, P., Nilforoushan, F., Hatzfeld, D., Abbassi, M. R., Vigny, C., Masson, F., … Chery, J. (2004). Present-day crustal deformation and plate kinematics in the Middle East constrained by GPS measurements in Iran and northern Oman. *Geophysical Journal International*, *157*(1), 381–398. https://doi.org/10.1111/j.1365-246X.2004.02222.x

Vigny, C., Socquet, A., Rangin, C., Chamot-Rooke, N., Pubellier, M., Bouin, M., … Becker, M. (2003). Present-day crustal deformation around Sagaing fault, Myanmar. *Journal of Geophysical Research*, *108*(B11), 2533. https://doi.org/10.1029/2002JB001999

Walpersdorf, A., Hatzfeld, D., Nankali, H., Tavakoli, F., Nilforoushan, F., Tatar, M., … Masson, F. (2006). Difference in the GPS deformation pattern of North and Central Zagros (Iran). *Geophysical Journal International*, *167*(3), 1077–1088. https://doi.org/10.1111/j.1365-246X.2006.03147.x

Walpersdorf, A., Manighetti, I., Mousavi, Z., Tavakoli, F., Vergnolle, M., Jadidi, A., … Sedighi, M. (2014). Present-day kinematics and fault slip rates in eastern Iran, derived from 11 years of GPS data. *Journal of Geophysical Research: Solid Earth*, *119*, 1359–1383. https://doi.org/10.1002/2013JB010620

Wang, Q., Zhang, P.-Z., Freymueller, J. T., Bilham, R., Larson, K. M., Lai, X., … Chen, Q. (2001). Present-day crustal deformation in China constrained by Global Positioning System measurements. *Science*, *294*(5542), 574–577. https://doi.org/10.1126/science.1063647

Xu, Y.-G., Wei, X., Luo, Z.-Y., Liu, H.-Q., & Cao, J. (2014). The Early Permian Tarim Large Igneous Province: Main characteristics and a plume incubation model. *Lithos*, *204*, 20–35. https://doi.org/10.1016/j.lithos.2014.02.015

Yin, A. (2009). Cenozoic tectonic evolution of Asia: A preliminary synthesis. *Tectonophysics*, *488*(1-4), 293–325. https://doi.org/10.1016/j.tecto.2009.06.002

Yin, A. (2006). Cenozoic tectonic evolution of the Himalayan orogen as constrained by along-strike variation of structural geometry, exhumation history, and foreland sedimentation. *Earth-Science Reviews*, *76*(1–2),1–131.

Zarifi, Z., Nilfouroushan, F., & Raeesi, M. (2013). Crustal stress map of Iran: Insight from seismic and geodetic computations. *Pure and Applied Geophysics*, *171*(7), 1219–1236. https://doi.org/10.1007/s00024-013-0711-9

Zhang, P.-Z., Shen, Z., Wang, M., Gan, W., Bürgmann, R., Molnar, P., … Xinzhao, Y. (2004). Continuous deformation of the Tibetan Plateau from global positioning system data. *Geology*, *32*(9), 809–812. https://doi.org/10.1130/G20554.1

Zhao, J. M., Yuan, X., Liu, H., Kumar, P., Pei, S., Kind, R., … Wang, Q. (2010). The boundary between the Indian and Asian tectonic plates below Tibet. *Proceedings of the National Academy of Sciences of the United States of America*, *107*(25), 11,229–11,233. https://doi.org/10.1073/pnas.1001921107